$^{40}Ar/^{39}Ar$ dating

The $^{40}Ar/^{39}Ar$ stepheating method uses a series of apparent ages to recover possible crystallization ages for igneous rocks, and the reproducibility of the resulting step ages require the data to meet a basic mathematical requirement (Marzoli *et al.* 1999; Baksi 2003). The Mean Square Weighted Deviation (MSWD = *F*, Wendt & Carl 1991) value of plateau sections of age spectra are assessed for their probability of fit (*p*) using the number of steps involved and Chi Square Tables (Baksi 2012). The plateau is statistically valid only when $p > 0.05$ (Baksi 2003) or a more rigorous evaluation of $p > 0.15$ (Sharp and Clague, 2006). In Tarim, since 1996, twenty-four $^{40}Ar/^{39}Ar$ ages have been published for mafic and silicic rocks from outcrops and drill cores, with 20 ages having published raw data (Table 1). Only one of these is an age from dating feldspar, all the rest are whole-rock ages. There have been some previous attempts at compiling and evaluating this data (Li *et al.* 2011; Qin *et al.* 2011; Wei *et al.* 2014), but those datasets were not comprehensive, and the methods applied are subjective. We present a compilation of all known $^{40}Ar/^{39}Ar$ ages for Tarim, and evaluate their quality. We recalculate MSWD values of age spectra and corresponding *p* values of all $^{40}Ar/^{39}Ar$ ages using published raw data (Table 1).

Alteration in basalt lavas older than a few million years has been widely recognized (e.g. Karoo, Duncan *et al.* 1997; Deccan, Baksi 2014a), and even young basalt can be affected by alteration (e.g. alkali basalts from Hawaii, 780ka, Baksi *et al.* 1992). Alteration of undisturbed igneous whole-rock material used for argon dating usually results in inaccurate estimates of the crystallization age (Baksi 2007a, b). To quantify alteration state of basaltic groundmass and crystals for $^{40}Ar/^{39}Ar$ dating, Baksi (2007 a, b) introduced the calculation of Alteration Index (A.I.) value, which is $[(^{36}Ar/^{39}Ar)_M - (^{36}Ar/^{37}Ar)_{Ca} \times (^{37}Ar/^{39}Ar)_C] \times (J/0.01) \times (B/D)$, where $(^{36}Ar/^{37}Ar)_{Ca} = 0.00025$, D = 0.65% for whole rock material and D = 10.0% for feldspar, B is the K content (%) of basalt, see Baksi (2007a, b) for details. For ratios corrected for interfering reactions (e.g. YG-2 and

YG-14), we use a simplified equation for A.I. = ($^{36}Ar/^{39}Ar$) × (J/0.01) × (B/D) (Baksi pers. comm. 2014). Fresh material is defined as having A.I. < 0.00060. Such an approach has proved successful in evaluating the alteration state of $^{40}Ar/^{39}Ar$ dating of basalts in some continental flood basalts provinces (e.g. Columbia River Group, Baksi 2013; Deccan, Baksi 2014a; Siberian Trap & Emeishan flood basalt, Baksi 2014b). In the Emeishan flood basalts, Baksi (2014b) tested the proposed temporal link between such magmatic events with Permo-Triassic boundary mass extinctions (Lo *et al.* 2002). However, all five whole rock samples in Lo *et al.* (2002) are determined to be quite altered by the A.I. method (Baksi 2014b). To further quantify whole rock $^{40}Ar/^{39}Ar$ dating results in Tarim, we utilize this method to calculate the A.I. value of these dated basalts (Fig. 1a, Table 1).

Critical inspection of both mathematical validity and alteration state shows that only plateau ages of 281.8 ± 4.2 Ma from Yg20-21 (Yang *et al.* 2006a), 282.90 ± 1.55 Ma from LKC07-1 (Zhang *et al.* 2010a) and 277.5 ± 1.3 Ma from XH-8 (Yang *et al.* 1996) are statistically valid. However, Yg20-21 is based on only three steps with 35.82% ^{39}Ar released, which by definition, cannot constitute a plateau. LKC07-1, which has the most statistically robust plateau, shows severe alteration (Fig. 1a). The robust plateau could be the result of argon system resetting by the later thermal event (e.g. Baksi 2014b). Most published groundmass matrix samples were totally altered, with some steps from YG - 2 and YG - 14 (Wei *et al.* 2014) falling in the fresh zone. With only the steps in fresh zone, we calculate the MSWD and p value separately, and get MSWD = 18.59 with $p \approx 0$ for YG-2, and MSWD = 7.47 with $p \approx 0$ for YG-14. Therefore, no plateau age can be derived. In summary, except for XH-08 which has incomplete raw data, no $^{40}Ar/^{39}Ar$ data meets the requirements of mathematical validity and alteration state simultaneously. Many ages that appear to show plateau are drawn at scales that minimize variation (e.g. YG-2 and YG-14 in Wei *et al.* 2014). Originally, YG - 2 and YG - 14 were drawn at 120 to 400 Ma scale, but when redrafted as 270 Ma to 310 Ma and 274 Ma to 302 Ma, respectively, the apparent plateau show increased variability (Fig. 1b, 1c).

Zircons from basalt

Through new experimental petrology, Boehnke *et al.* (2013) have shown that high concentrations of Zr (> 5000 ppm) are required to directly crystallize zircon from basaltic liquids under simulated physicochemical conditions (1 GPa, 1175-1225 ℃). Previous geochemical studies of the Keping and Damusi basalt have found Zr concentrations < 500 ppm (191~495 ppm, Jiang *et al.* 2004a; 232~289 ppm, Yu 2009; 232~421 ppm, Yu *et al.* 2011b; 266~357 ppm, Zhou *et al.* 2009; 330~402 ppm, Damusi basalt, Li *et al.* 2008). Therefore, it seems unlikely that zircons crystallized from these basalts.

Hf isotope data of KZ basalts in Keping have been reported by Li (2013). Though the age of KZ basalt is still unclear, we calculate the εHf(t) back to the age of the zircon, and get εHf(t) value from -2.17 to +2.26, calculated at 300 Ma, and from -2.48 to +1.96, calculated at 280 Ma. Li *et al.* (2012) reported Hf isotope data on Keping basalts; however, the raw data did not contain $^{176}Lu/^{177}Hf$ values, and therefore cannot be recalculated. So we do not use this data. The εHf(t) of zircon from Keping basalt, calculated for the age of each grain, shows a range of -6.8 to -1.1. Most zircons (82%, 29 out of 34) have εHf(t) less than -2.48 (Fig. 2a), which is the minimum εHf(t) value in equilibrium with Keping Basalt. The highly negative values of most zircons compared to host basalt further suggests the bulk of zircons are not crystallized from the basalt they are found in. The low Zr concentration and low εHf(t) suggest that the zircons are not likely directly crystallized from the host Keping basalt.

Three possible processes can lead to the incorporation of zircon xenocrysts: (1) zircons incorporated into lavas during post-eruptive flow over zircon bearing sediments; (2) assimilation of zircon-bearing wall rocks in the magma chamber; (3) assimilation of zircon-bearing rhyolitic melt that may be cogenetic with basalt.

If zircons come from a post-eruptive sedimentary origin, the zircon population will reflect the characteristics of the zircon in the underlying sedimentary unit. Data from sandstones underlying both KZ basalt and interlayered with KZ basalt (Zou *et al.* 2013), and sandstones underlying and overlying Qimugan basalt (Li at el., 2013) show a distinctive and much more complex population than the basalt zircons (Fig. 3b and 3c). Most of the zircons from basalt have ages less than 300 Ma (80%), whereas zircon in sandstones have only 14 to 52 % of grains younger than 300 Ma (Fig. 3a), and extend to 2.78 Ga. Also, it is worth noting that the basalt zircons have a significant restricted ages of 290 to 300 Ma, which constitutes 36 %. Three Keping sandstones have only 5 to 12 % of 290 to 300 Ma age zircons, and the 290 to 300 Ma population is nearly absent in the Damusi sandstones (Fig. 3a, 3b).

Some researchers (e.g. Sircombe 1999; Berry *et al.* 2001) argue that the visual comparison of age spectra or histograms of detrital zircon data could be subjective. Some statistical approaches such as the Kolmogorov-Smirnoff test (K-S test) have been adapted to mathematically compare two age distributions and determine if there is a statistically significant difference between them (Berry *et al.* 2001). The fundamental criterion of the K-S test is p: if p is less than 0.05, there is a > 95% confidence that the two age distributions are different (Berry *et al.* 2001). Following this approach, we make a K-S test for all the basalt zircon single grain ages (n = 118) versus detrital zircon single grain ages from three Keping sandstone layers (Yg050409, n = 52; Yg050412, n = 82 and Yg050413, n = 83 from Zou *et al.* 2013, after eliminating the discordant ones), to determine if there is a statistically significant difference between the basalts and each sandstone. We get p value of 0.000, 0.000 and 0.026 for each comparison. Therefore, the main source of basalt zircon does not appear to be related to sediments intercalated with the lavas.

If zircon was incorporated from wall rock during magma ascent, the basalt should assimilate material captured from the wall rock other than zircon crystals, which will undoubtedly lead to crustal contamination of the magma. The population density of zircon from 11 different layers of Keping basalt is around ~44 grains per kilogram (from 13 to 104, with standard deviation = 24). The population density of zircon from two Halahatang rhyolite samples is > 3000 grains per kilogram. An average of 15 g of rhyolite will supply 1 kg of basalt with 45 zircon grains, which means that mixing of ~ 1.5% rhyolitic magma would be sufficient to serve as a source for zircon xenocrysts in basalt magma, and such a small amount of assimilation would not significantly impact major element geochemistry. The strong 290 to 300 Ma zircon signature rules out the possibility of sourcing basement zircon from the Tarim Carton, which has experienced eight main phases of tectothermal events from 2950 to 400 Ma (Wu *et al.* 2012). Therefore, assimilation of zircon-bearing rhyolitic material appears to be the most likely source of basalt zircons, and the occurrence of intercalated rhyolites within the basalt lavas suggests that silicic and basaltic magmas could have interacted.

Li *et al.* (2014) suggested that the Keping basalt zircons were probably from coeval silicic volcanic and pyroclastic rock suites (VPR suite) in the South Tianshan Orogen based on the zircon Hf isotope similarity, morphological characteristics and Th/U ratios. Hf isotopes do discriminate between different components of Tarim volcanism, and suggest a correlation between zircons from basalts and the VPR suite. The Th/U ratio is not a good discrimination tool, and all Tarim zircons overlap (Fig. 2b). Since zircon in basalt are not likely entrained after eruption, the most likely possibility is pre-eruption assimilation. Considering that Keping basalt is more than 300 km away from dacite outcrops in Tianshan, we propose that any genetic linkage between possible zircon source and basalt magmas requires more constraints. Also, while the zirconium saturation criteria of Boehnke *et al.* (2013) indicates that Keping basalts will not crystallize zircon, the Watson & Harrison (1983) calculations used by Li *et al.* (2014) are only applicable to silicic compositions.

Silicic extrusive and intrusive rocks

In general, for silicic rocks we recalculate the error correlation (RHO value) of $^{207}Pb/^{235}U$-$^{206}Pb/^{238}U$ ratios, and ages with RHO beyond the range of 0 to 1 are eliminated. We interpret the zircon grains corresponding to discordant dates to be affected by lead loss. However, the lead loss in zircon has several possible causes that are difficult to quantify (e.g. radiation damage, diffusion, Mezger & Krogstad 1997), and the high temperature annealing of zircon makes such issues even more complex (Cherniak & Watson 2001). Detailed CL imaging analysis will help to identifying the metamict zircons, which are highly likely to have lead loss. However, such data are rarely available in previous Tarim studies. Therefore, a more robust scheme for dealing with lead loss is to not use any zircon data that potentially suggests lead loss (Schoene 2014). The strategy we applied here is generally avoiding the discordant dates.

Xiaohaizi syenite intrusion

The Xiaohaizi syenite intrusion, also referred to as the Mazhartage syenite intrusion, is located in the Bachu uplift on the northwest margin of the Tarim basin (Fig. 4). This syenite body is circular in shape, with a radius of ~2.5 km. It is overprinted by a more laterally extensive network of mafic dykes and quartz syenite porphyry dykes that extent for tens to hundreds of meters in length, with widths of 0.6 to 4 m (Zhang *et al.* 2008b). While there has been a lot of geochronologic work on this system, the outcrop geology is not well constrained. The most recent publications bases their geologic map on remote sensing data and field work (Zhang *et al.* 2008b). Original mapping divided the intrusion into syenite and gabbro (Jiang *et al.* 2004c; Yang *et al.* 2006b, 2007; Sun *et al.* 2008). Sun *et al.* (2009) divided the intrusion into pyroxene syenite and amphibole syenite. Recently, Chen *et al.* (2010), Wei & Xu (2011, 2013), Xu *et al.* (2014) followed the map of Zhang *et al.* (2008b), which divides the intrusion into syenite, quartz syenite and olivine gabbro. Wei & Xu (2011) also reported the occurrence of fayalite syenite and amphibole syenite; however, the field relations remain complex because the extreme topography restricts detailed mapping.

Eight zircon U-Pb ages, one whole rock (?) Ar-Ar age and one K-Ar age have been reported on multiple lithologies from many different parts of the syenite intrusion (Table 2). Excluding the K-Ar age, which does not have raw data, the ages range from 285.9 ± 2.6 Ma to 273.7 ± 1.5 Ma (Table 2).

We recalculate every age using the published raw data and redraw every U-Pb concordia plot (Fig. 5a). After eliminating spots with RHO (correlation coefficient, e.g. Ludwig 1998, Schmitz & Schoene 2007) values out of the 0 to 1 range, which implies that the uncertainty in the $^{207}Pb/^{206}Pb$ ratio is a significant source of dating (Mattinson 1987), or visually away from concordant curves, we get an average total age of 279.8 Ma, with individual sample ages ranging from 285.2 ± 3.6 Ma (95 % conf.) to 272.3 ± 7.3 Ma (95% conf.) (for details of recalculation, see Table 2 caption). Some important changes occur compared to the original data, and will be discussed. Yang *et al.* (2006b) analyzed 15 zircons from one sample by SHRIMP U-Pb method, they eliminated four ages (253.7, 254.3, 301.7 and 248 Ma) and got a weighed mean average age of 277 ± 4 Ma. We repeated his calculation with raw data from the rest 11 spots be used and get a weighted mean average age of 271.4 ± 3.7 Ma. However, Yang *et al.* (2006b) did not justify why the four ages should be thrown out, so we include them here because they are concordant and appear robust. The new weighed mean average age of all the 15 zircons is 272.3 ± 7.3 Ma (95% conf.). All the spots in Zhang *et al.* (2008a) have negative RHO value, indicating some issues with these data. Also, in Sun *et al.* (2008), the percentage error of $^{207}Pb/^{235}U$ ratio is notably one magnitude larger than that of $^{206}Pb/^{238}U$, which results in fairly flat concordia plots (Fig. 5a).

Based on our recalculation of all of the Xiaohaizi syenite data, the ages are 285.2 ± 3.6 Ma to 272.3 ± 7.3 Ma (Table 2, Fig. 6b), with an age span totaling 12.9 Ma and standard deviation of 4.3 Ma. The LA-ICP-MS zircon dating usually has a precision of 1 %

to 8 % for individual spot analyses, whereas SHRIMP and SIMS could be <5 %. The difference between the oldest and youngest syenite ages equals ~4.7 % of the youngest age, and so all of this difference could be attributed to analytical errors. However, due to the lack of accurate geology mapping and precise sample location, it's difficult to conclusively assess the source of the age data scatter. It is possible that the large diversity of composition reflects long-lived magmatism, and this may be producing the observed age range.

The reported dating material includes syenite, quartz syenite, pyroxene syenite and amphibole syenite (Table 2). To evaluate the possible diversity of igneous rocks, we checked reported mineral assemblages of each sample. Some are mafic and olivine-bearing, while others have quartz present, at up to 30 % by volume (Table 2). Also, for three ages with published geochemistry data and additional geochemistry from Zhang *et al.* (2008a), major element compositions vary dramatically, e.g. SiO_2 ranges from 58.59 % to 69.07 % (Fig. 6a). By using a K-means approach to cluster the composition groups, we cluster the 28 published data into four groups by SiO_2-MgO-CaO content. The center of each group is shown in Fig. 6a, with SiO_2 content of 60.98%, 63.53%, 65.29% and 68.12%, respectively. In summary, both the mineral assemblages and major element data suggests a complex syenite intrusion, which requires more detailed study to fully understand.

Long-lived syenitic centers are reported in East Greenland, which are interpreted to be genetically linked to the North Atlantic Igneous Province (NAIP), and have an age span of ~10 Ma (Riishuus *et al.* 2006). These systems contain a variety of lithofacies including syenites, granites, quartz syenites and nepheline syenites, and displays a temporal evolution in which SiO_2 decreases with younging (74-56 %, Riishuus *et al.* 2006). Similarly, we note that the three ages linked to geochemistry data in the Xiaohaizi syenite intrusion also show a positive correlation between age and SiO_2 content (Fig. 6a).

Granite plutons

The Halajun area of northwest Tarim has eight granites (Fig. 7), two of which are dated by SHRIMP U-Pb on zircon grains (Halajun 1 and Halajun 2), and the remaining six by LA-ICP-MS U-Pb on zircon grains. The results range from 278 ± 3 Ma to 268.6 ± 1.5 Ma (Zhang *et al.* 2010a; Huang *et al.* 2012; Zhang & Zou 2013). We recalculate every age using the published raw data and redraw every U-Pb concordia plot (Fig. 5b).

For the Halajun 1 pluton, Zhang *et al.* (2010a) obtained 14 analyses, and data point 1.1 (289.8 ± 10.9 Ma) was eliminated due to its large error (Zhang *et al.* 2010a). However, the large error of $^{206}U/^{238}Pb$ age is not reason enough to eliminate data. We made a concordia plot for this pluton and find that data point 1.1 as well as 4.1 lie off of the concordance line. For this reason, we eliminate these two data points, and get a weighted mean average age of 274.6 ± 2.2 Ma.

For the Halajun 2 pluton, Zhang *et al.* (2010a) obtained 17 analyses, with data point 1.1 (569.1 ± 10.7 Ma) being eliminated for having an old age and obvious bigger grain size (Zhang *et al.* 2010a). On a concordia plot, it is clear that all the data points lie off the concordance line, with the exception of point 1.1. However, this age is significantly older than all the other ages from surrounding plutons, and without additional data it is difficult to evaluate the geological context. So, we do not consider it further here.

For the Halajun 3 pluton, Zhang & Zou (2013) obtained 20 analyses, within which 8.1 (515.1 Ma), 9.1 (337.3 Ma) and 15.1 (293.2 Ma) were eliminated for variably older ages, and in addition 8.1 and 9.1 have much larger grain sizes. The remaining 17 data points yielded a weighted mean average age of 271 ± 2 Ma with an MSWD = 8.5. Considering the high MSWD, the author further eliminated zircons 6.1 (284.1 Ma) and 12.1 (280.7 Ma) to get a new age of 268.6 ± 1.5 Ma with a lower MSWD (1.6). However, no justification was given for why these addition ages were eliminated. Analyses 6.1, 8.1 and 9.1 have $^{207}U/^{235}Pb$ ratio and $^{207}U/^{235}Pb$ ratios one magnitude larger than other data points, which indicate a significant excess of ^{207}Pb, and lie far off the concordance line. In addition, the corresponding error of $^{207}U/^{235}Pb$ ratio for analysis 9.1 is one magnitude larger than other data points, and yields RHO > 1. Also, 12.1 and 15.1 are off the concordance line due to relatively higher $^{207}Pb/^{235}U$ and $^{206}Pb/^{238}U$ ratio respectively. After eliminating these five analysis, we get a weighted mean average of 268.6 ± 2.0 Ma.

For the Halajun 4 pluton, Zhang & Zou (2013) obtained 20 analyses, and eliminated 5.1 and 6.1 for their significantly younger ages, which they attributed to inclusions in zircon grains observed in transmitted photos. Analyses 5.1 and 6.1 have RHO value 1.01 and -0.59 respectively, which indicate something may be impacting the covariation of $^{207}Pb/^{235}U$ and $^{206}Pb/^{238}U$, and the existence of inclusions would be a reasonable explanation. In addition, 13.1 also has a negative RHO (-0.13) value, and may also contain inclusions. On a concordia plot, 17.1 is one magnitude larger in error for the $^{207}Pb/^{235}U$ and $^{206}Pb/^{238}U$ ratios, which may be due to the low U concentration (23 ppm), and may cause larger uncertainty in the age calculation. Analyses 18.1 is off the concordance line due to its high $^{207}Pb/^{235}U$ ratio. After eliminating these five data points (5.1, 6.1, 13.1, 17.1 and 18.1), the remaining 15 data points yield a weighed mean average age of 268.7 ± 1.6 Ma.

For the Halajun 5 pluton, Zhang & Zou (2013) obtained 20 analyses, with 3.1, 5.1, 8.1 and 12.1 being eliminated for their younger ages, and the authors attributed these four younger zircons to metamictization. The reported absolute error of $^{207}Pb/^{206}Pb$ ranges from 2.01 to 3.62, with $^{207}Pb/^{206}Pb$ ratio from 0.0053 to 0.0115, and absolute error of $^{207}Pb/^{235}U$ ratio is from 0.1857 to 0.3386, with $^{207}Pb/^{235}U$ ratio from 0.8 to 1.25. Therefore the percentage error would be more than 30,000% for $^{207}Pb/^{206}Pb$ and ~ 35% for $^{207}Pb/^{235}U$.

For the Kezile pluton, Zhang & Zou (2013) obtained 25 analyses (note that the published data listed as Kezile does not correspond to the plot for this pluton. We use the table data as correct. On a concordia plot, all the analysis are concordant, and yield a weighted mean average age of 268.7 ± 1.6 Ma, with MSWD of 0.94.

For the Guerlale pluton, Zhang & Zou (2013) obtained 17 analyses. Three analyses have distinctive higher $^{207}Pb/^{206}Pb$ ratios than other analyses, with two of them (3 and 15) off the concordance line and, one (10) with a negative RHO value. Analyses 2 and 10 also have negative RHO values, which indicate a proportional negative variation between $^{207}Pb/^{235}U$ ratio and $^{206}Pb/^{238}U$ ratio, which can be further confirmed by their old $^{207}Pb/^{235}U$ ages (523 Ma and 420 Ma, respectively). Analyses 16 has an age of 257 ± 1 Ma, and is concordant without any evidence of lead loss or anomaly in experiment. However, it is distinctively younger and does not overlap with any other single grain age from the surrounding plutons within 1σ error, so we do not use it in the weighted mean average age calculation. The remaining 13 analyses yield an age of 271.4 ± 1.6 Ma.

For the Kezi'ertuo pluton, Huang *et al.* (2012) obtained 35 analyses, and all the analyses are concordant, and yielded an age of 272.7 ± 1.1 Ma (Table 3, Fig. 5b).

After recalculation, the ages for Halajun plutons range from 275.3 ± 1.1 Ma to 268.6 ± 2.0 Ma, with an age span of 6.7 Ma (Fig. 6c). It should be noted that the single zircon ages of the Kezile and Guerlale plutons show age ranges of 11 Ma and 9 Ma, respectively, and have high MSWD values of 3.6 and 5.5. This suggests that the zircons reflect a complex magmatic history. Several distinctive zircon populations can be recognized on the weighted mean average plot for the above two plutons (Fig. 8a and 8b). In addition, granites with relatively low MSWD also show large spans between the oldest and youngest grains. For example, Halajun 4 pluton has a span of 15.3 Ma, from 275.9 Ma to 260.6 Ma (Fig. 6c).

Advances in zircon TIMS and SIMS analyses result in reduced analytical uncertainty. Studies have shown that the timeframe of granitic pluton assembly is potentially several million years (e.g. > 5 Ma for Mt. Stuart, WA., USA; > 8 Ma for Tuolumne, CA., USA; Miller *et al.* 2007). The granitic plutons presented here could be characterized by continuous or episodic growth and the dating of granite emplacement could also be complicated by multi-stage growth of zircon. Possible approaches to address such complexity could be coupled back-scattered electron (BSE) and cathodoluminescence (CL) imaging with chemical analyses of zircon (e.g. Gagnevin *et al.* 2010).

For all granite plutons, only one concordant age is distinctively older than other single grain ages (1.1 of the Halajun 2 pluton: 569.1 Ma). There appears to be a notable lack of xenocrystic zircons in these plutons, for xenocrysts would presumably have to be appreciably older than the majority of zircon crystals. Considering the big age scatter in individual plutons in this area, it is more likely that the majority of zircon populations either grew continuously or sporadically within these magmas.

Miller *et al.* (2003) observed a suite of fifty-four granitoids, and found that the plutons with a lot of inherited zircons usually have Zr saturation temperature (T_{zr}) < 800 ℃ and those without have T_{zr} > 800 ℃. (Tzr is calculated using the empirical equation by Watson & Harrison 1983). It is intriguing that the granite plutons in the Halajun area show variable MSWD value, from 5.5 to 0.74. The lack of published zircon CL images of these plutons makes it impossible to identify different zircon population by morphological characteristics. So, to attempt to quantify the extent of inherited zircons, we calculated the standard deviation (SD) of single zircon ages of individual plutons instead of using the MSWD value. Because some analyses were done by LA-ICP-MS and some by SHRIMP, we cannot directly compare MSWD. We calculate the T_{zr} of the six granite plutons with concordant ages, and find that a negative correlation (Fig. 6d). Fitting curve: standard deviation = -0.0303 T_{zr} + 29.854) can be observed between T_{zr} and standard deviation. Following the interpretation of Miller *et al.* (2003), we propose that the preservation of inheritance is reflected by T_{zr} values. The higher T_{zr} values, such as Kezi'ertuo, indicate increasingly zirconium undersaturated melt which do not support the preservation of older zircons. The lower T_{zr} values, such as Halajun 3, indicate the more saturated melts, which are not prone to dissolve previous zircons, and therefore will have higher inheritance. The remaining four granites plot at intermediate T_{zr} values and may have some inherited zircons. This is reflected in the decreasing scatter of single zircon ages of these plutons with increasing T_{zr}.

Silicic extrusive rocks

Rhyolite and dacite silicic extrusive rocks are widely reported in drill core in northern Tarim (e.g. Shun and Yingmai drilling area, Yu *et al.* 2011a; Tian *et al.* 2010) and Wenquan outcrop by the north margin of Tarim (Liu *et al.* 2014). Five rhyolites have been dated, three of which were done by zircon U-Pb LA-ICP-MS method, one by zircon U-Pb SHRIMP, and one by zircon U-Pb CA-TIMS (Table. 4; Tian *et al.* 2010; Liu *et al.* 2014), with an age range of 290.9 ± 4.1 Ma to 271.7 ± 2.2 Ma. Seven dacite ages have been reported, all of which were done by zircon U-Pb LA-ICP-MS (Li *et al.* 2007; Zhang *et al.* 2009; Tian *et al.* 2010; Yu *et al.* 2011a), with an age range of 286.6 ± 3.3 Ma to 273.7 ± 3.2 Ma.

We recalculated every age using the published raw data, and find that both the data quality and interpretation of one rhyolite SHRIMP age and four rhyolite (or dacite) LA-ICP-MS ages in Tian *et al.* (2010) are good. All the four dacite LA-ICP-MS ages in Yu *et al.* (2011a) have underestimated MSWD values, which should be 1.76 for S102-1, 1.69 for S114, 1.78 for S79-3 and 1.73 for S99. For the remaining two LA-ICP-MS data, the authors showed rather convincing reasons for eliminating discordant data points and obvious xenocrysts (Li *et al.* 2007; Zhang *et al.* 2009). While the remaining data are concordant, they exhibit single grain ages that span more than one magnitude bigger than single grain errors (1σ) and exceed 15 % of the weighted mean average age (e.g. 57 Myr span for Shun 1 in Li et al. 2007; Fig. 8c). The continuous zircon age distribution reflects a complex magmatic process, which could be attributed to continuous magma recharge and accompanying zircon crystallizat ion (e.g. Miller *et al.* 2007). Therefore the significance of the weighed mean average age will be ambiguous. So, such data could only provide a relatively loose constraint on emplacement time of the rhyolite or dacite.

Recently, Liu *et al.* (2014) reported a zircon U-Pb CA-TIMS age of Wenquan rhyolite (WQ09-2) of 286.8 ± 0.5 Ma (95% conf., MSWD = 2.0). Given the high MSWD value, it is obvious that the variability in single grain ages cannot be explained by analytical scatter alone (Wendt & Carl 1991; Schoene *et al.* 2013). In the consideration of high precision of TIMS dating, scientists usually regard the observed age scatter which is more than one magnitude bigger than the analytical error as the involvement of antecrystic zircons, and use the weighted mean age of statistically equivalent youngest population (e.g. Michel *et al.* 2008; Memeti *et al.* 2010) or the youngest single grain age (e.g. Schaltegger *et al.* 2009; Schoene *et al.* 2010; Barboni *et al.* 2013) to estimate the timing of magma emplacement, and the former approach is presumably more conservative. The data from Liu *et al.* (2014) could be interpreted as at least two distinct groups, with the youngest four analyses and oldest three analyses having weighted mean average ages of 287.56 ± 0.71 Ma (95% conf., MSWD = 0.039) and 284.20 ± 1.60 Ma (95% conf., MSWD = 0.074) (Fig. 8d). The 3.36 million year (>1 %) age gap is one magnitude larger than the expected precision of zircon U-Pb CA-TIMS method, which should be better than 0.1 % (Mattinson 2005). Therefore, we consider it to be real and reflect different populations of zircons. The youngest single grain age is 283.4 ± 7 Ma, which is overlapped with the youngest population (284.20 ± 1.60 Ma) within analytical error. We interpret the oldest population (287.56 ± 0.71 Ma) as recording the oldest identifiable magmatic activity, and adopt the youngest population (284.20 ± 1.60 Ma) as recording late-stage crystallization, which could be the best approximation of eruption age.

Silicic dykes

Silicic dykes are reported in the Xiaohaizi and Wajilitag area, including quartz syenitic porphyry (Zhang *et al.* 2008b; Yu 2009; Li *et al.* 2011; Fig. 4), potash-feldspar-granite vein (Sun *et al.* 2009) and granodiorite (Zhang *et al.* 2009). The potash-feldspar-granite vein for geochronology study intruded into the Xiaohaizi syenite intrusion (Sun *et al.* 2009), the samples in Chen *et al.* (2010) and Li *et al.* (2011) were taken from the quartz syenitic porphyries that intrude into sediments, the contact relationships of granodiorite in Zhang *et al.* (2009) study was not clearly documented.

In the Xiaohaizi area, Yu (2009) reported zircon U-Pb SHRIMP dating of quartz syenitic porphyry, which is 278.4 ± 2.2 Ma. By recalculating and plotting and their raw data, we propose that one analysis is discordant (analysis 10.1) among the total thirteen, and the remaining data yield a weighted mean average age of 279.2 ± 2.5 Ma. At least two distinctive age groups can be recognized, indicating possible prolonged or complex magmatic processes (Fig. 8j). Sun *et al.* (2009) reported zircon U-Pb LA-ICP-MS result of potash-feldspar-granite vein, which had eleven analysis, and yielded a weighted mean average age of 282.0 ± 3.7 Ma. Li *et al.* (2011) reported zircon U-Pb SHRIMP results of a quartz syenite porphyry, and got a weighted mean average age of 284.3 ± 2.8 Ma. It should be noted that the error of the $^{207}Pb/^{235}U$ ratio is one magnitude higher than the error of the $^{206}Pb/^{238}U$ ratio, which is shown by the compressed error ellipses in the concordia plot, and this may due to the low concentration of ^{207}Pb or experimental issues (Fig. 5d). In the Wajilitag area, Zhang *et al.* (2009) reported forty-one analyses of zircon by the U-Pb LA-ICP-MS method for granodiorite, with an age of 295.9 ± 2.1 Ma. We recalculate and replot the raw data (Fig. 5d), and get a weighted mean average age of 295.8 ± 1.8 Ma, with MSWD = 2.1. Based on the data we have, the silicic dykes in Xiaohaizi area are younger than Wajilitag granodiorite, despite their close proximity. In summary, the silicic dykes have a narrower age range than the mafic dykes, and the linkage of the silicic dykes in the Xiaohaizi and Wajilitag areas requires more constraint.

Detrital zircon ages

The detrital zircon data from sedimentary rocks intercalated with Tarim volcanism has only just started being investigated. Recently, Zou *et al.* (2013) dated the detrital zircons from three sandstone layers underlying and interbedded with the KZ Fm basalt, and Li *et al.* (2013) carried out detrital zircon age dating from three sandstone layers underlying and overlying the Qimugan basalt (Fig. 3a, 3b and 3c). Both of their interpretations were restricted to simply using the weighted mean average age of the youngest population to constrain the maximum depositional age of the sandstone, and in turn to constrain the maximum emplacement age of the overlying basalt (Fig. 3c). However, their selection of the youngest zircon populations require more explanation.

Dickinson & Gehrels (2009) tested four alternate measures of youngest detrital zircon ages (mainly dated by LA-ICP-MS) using sediments from the Colorado Plateau with depositional ages known independently by biostratigraphy. They proposed the four measures, from least to most statistically robust, as follows: (a) youngest single grain age (YSG), (b) youngest graphical age peak controlled by more than one grain age (YPP), (c) mean age of the youngest two or more grains that overlap in age at 1σ (YC1σ(2+)), and (d) mean age of the youngest three or more grains that overlap in age at 2σ (YC2σ(3+)). We use these four measures to reevaluate the maximum depositional ages of the sandstones presented in Zou *et al.* (2013) and Li *et al.* (2013), and the results are shown in Table 6.

For the Yg050409 sample in Zou *et al.* (2013), the YSG age (244 ± 3 Ma) is significantly younger (> 10 Ma) than the other three corresponding ages (YPP: 270.7 Ma, YC1σ(2+): 255.3 ± 2.6 Ma, YC2σ(3+): 263.7 ± 3.9 Ma), as well as the second youngest grain (253 Ma). This could be interpreted as contamination from a younger source. The second youngest single grain age is 253 ± 2 Ma, and is in accordance with YC1σ(2+) age (255.3 ± 2.6 Ma). The YPP age (263.7 Ma at chest) is compatible with YC1σ(2+) age (263.7

± 3.9 Ma). So we take ~263 Ma as a statistically robust estimate of the maximum depositional age of the host sandstone (Fig. 3b). Zou et al (2013) used 284 Ma.

For the Yg050412 in Zou *et al.* (2013), the YSG age (255 ± 3 Ma) is ~12 Ma younger than the other three corresponding ages (YPP: 267.7 Ma, YC1σ(2+): 267 ± 3.4 Ma, YC2σ(3+): 267 ± 3.4 Ma), as well as the second youngest grain (266 Ma), and could also be interpreted as contamination. The second youngest single grain age is 266 ± 3 Ma, which is in accordance with the YPP (267.7 Ma), YC1σ(2+) (267 ± 3.4 Ma) and YC2σ(3+) (267 ± 3.4 Ma) ages. Therefore, we take ~ 267 Ma as a statistically robust estimate of the maximum depositional age of the host sandstone (Fig. 3b). Zou et al (2013) used 287 Ma.

For the Yg050413 in Zou *et al.* (2013), the YSG age (247 ± 3 Ma) is more than 20 Ma younger than the other three corresponding ages (YPP: 278.2Ma, YC1σ(2+): 267 ± 4.2 Ma, YC2σ(3+): 276 ± 3.8 Ma), and 19 Ma younger than the second youngest grain (266 Ma) , which could be attributed to contamination as well. The second youngest single grain age is 266 ± 3 Ma, which is in accordance with YC1σ(2+) age (267 ± 4.2 Ma). The YYP age is 278.2 Ma and the YC2σ(3+) age of 286.7 ± 3.8 Ma contains twenty-one analyses , which is a robust but potentially conservative estimate of the maximum emplacement age of their overlying basalt (Fig. 3b). Zou et al (2013) used 291 Ma.

When all the data are compiled (217 analysis, excluding analyses off the concordance line), we calculate the YC1σ(2+) age of 255.2 ± 2.4 Ma representing five grains. An additional twenty grains are younger than 275 Ma, constituting 11.5 % of the total dates, and the YC2σ(3+) age of 282.4 ± 3.1 Ma is based on ninety grains.

Using the four measures they defined in their case study, Dickinson & Gehrels (2009) inferred that the YC2σ(3+) age is most likely to yield a result compatible with depositional age and also the most conservative measure among the above four measures. Following this interpretation, we propose that the three Zou et al (2013) samples have maximum depositional ages of 263.7 ± 3.4, 267 ± 3.4 and 287.6 ± 3.8 Ma.

Therefore, such maximum depositional ages of the sandstone require that the overlying basalts are younger or equal to those ages.

In Li *et al.* (2013), they reported the youngest population age for QMG1106 as 284 ± 4 Ma, which is in accordance with our calculation of the YSG, YPP, YC1σ(2+) and YC2σ(3+) ages, all of which are in the range of 285 to 284 Ma. In combination, this makes a robust constrain of the maximum depositional age at ~ 284 Ma. For QMG1112, the YC1σ(2+) age is based on the youngest group with two grains having a weighted mean average age of 268 ± 5.5 Ma and the YC2σ(3+) age is derived from the second youngest group with four grains having a weighted mean average age of 284.1 ± 4.7 Ma. We take the YC2σ(3+) age as the most conservative estimate of the maximum depositional age of the sandstone (Fig. 3b). In summary, the maximum emplacement age of Qimugan basalt is constrained by the maximum depositional age of the underlying sandstone at ~ 284 Ma.

Mafic dykes

Geochronology work have been carried out on mafic dykes from Xiaohaizi, Tangwangcheng and Wajilitag sections in the Bachu area, Yijianfang, Dawangou and Yingan sections in the Keping area, and two drill cores from Fang 1 and Yudong 2 well (Li *et al.* 2007; Zhang *et al.* 2009; Yu 2009; Zhang *et al.* 2010c; Liu *et al.* 2012; Wei & Xu 2013; Table 5). In the Xiaohaizi section, diabase dykes cut through some parts of the syenite body (Li *et al.* 2007; Zhang *et al.* 2010c; Wei & Xu 2013; Fig. 4); in the Tangwangcheng section, diabase intruded into carbonates of unknown age (Zhang *et al.* 2010c); in the Dawangou section, diabase dykes intruded into Silurian carbonates (Zhang *et al.* 2010c); in the Yingan sections, diabase dykes intruded into basalts (Yu 2009); and in the Yudong 2 well, diabase dykes intruded into carbonate (Liu *et al.* 2012). In Wajilitag and Yijianfang sections and Fang 1 well, no clear relationships between the dated gabbro dykes and the wall rock were described.

The mafic dykes in the Xiaohaizi area are believed to be derived from decompression melting of convecting mantle because of their OIB-like trace element signatures, and are interpreted as representing the later episode of the Tarim volcanism in the early Permian (Wei *et al.* 2014). However, the genetic link between mafic dykes in different locations is unclear, and some authors assumed these mafic dykes formed simultaneously and used them as a horizontal marker (e.g. Chen *et al.* 2009; Li *et al.* 2011).

Twelve ages of mafic dykes are reported, five of which were done by whole rock ^{40}Ar-^{39}Ar methods, with seven done by zircon U-Pb LA-ICP-MS SHRIMP and SIMS methods (Table 5). The whole rock ^{40}Ar-^{39}Ar dating results have already been discussed (see ^{40}Ar-^{39}Ar dating part). Yu (2009) reported zircon U-Pb SHRIMP result of six grains from diabase in the Yingan area with ages of 268, 290, 291, 753, 769 and 1133 Ma respectively. Similarly, Wei & Xu (2013) reported zircon U-Pb SIMS results of seventeen grains from diabase in the Xiaohaizi area, with ages range from 717 to 2390 Ma. Obviously, inherited zircons occur in the above two samples and complicate the interpretation, so we do not consider them further. The remaining five zircon U-Pb LA-ICP-MS ages range from 283.1 ± 3.2 Ma to 265 ± 16 Ma (Table 5), with an 18.1 million year age span.

Using the published raw data and replotting the five ages, we find that none of the ages for Xiaohaizi gabbro is robust (Fig. 5c). The Yijianfang gabbro from Li *et al.* (2007) and Yijianfang diabase from Zhang *et al.* (2009) both had a large number of discordant ages, and the remaining concordant ages have a large age span of ~ 25 Myr (Fig. 8e and 8g). The Wajilitag gabbro data from Zhang *et al.* (2009) also show big scatter, with concordant analyses having an age span of 75.4 Myr (Fig. 8i). No additional information can be applied to interpret the large age spans of the above three samples, so we propose that they cannot provide precise emplacement ages. One Xiaohaizi diabase sample from Li *et al.* (2007) yielded a weighted mean average age of 271.8 ± 5.8

Ma, with MSWD = 12 and 52 Myr age span (Fig. 8f). The big age span is probably affected by inherited zircon involvement, and the sample location and field relationship with the wall rock is unclear in the original source. Therefore, the geological significance of such age is lacking. One Xiaohaizi gabbro date from Zhang *et al.* (2009) yields a weighted mean average age of 282.9 ± 2.9 Ma, with MSWD = 3.6 and 30.6 Myr age span (Fig. 8h). In consideration of the prevalent inherited zircons in other mafic dykes we discussed above, we suggest this age could only be used for reference, and more work should be done to clarify the inherited zircon effect.

Zircon crystallizes in differentiated gabbroic environment and can be used to represent the crystallization age of host rock (e.g. Kaczmarek *et al.* 2008). However, zircons in mafic environment usually experience a complex history, which makes it necessary to identify zircon origins and group populations by variable approaches such as zircon chemistry and morphology (e.g. Grimes *et al.* 2009). The large age span here indicates the occurrence of different zircon populations either crystallized from or entrained by the mafic dykes. In summary, the ages of mafic dykes are still not well-constrained, and the assumption of homogeneity of mafic dykes in different locations is not supported by the current data.

In summary, the genetic link between geographically isolated (e.g. Yingan dyke is 150 km away from Xiaohaizi dyke) mafic dykes is unclear. Based on current data, it is unlikely that the mafic dykes were emplaced synchronously, although the large range in zircon ages makes this difficult to assess.

Kimberlite mineral U-Pb dating

Field relationships and chemistry

Ultramafic cryptoexplosive breccia has been reported in the Wajilitag region by a number of researchers (Du, 1983; Wang & Su 1987, 1990; Liang & Fang 1991; Su 1991; Li *et al.* 2001; Jiang *et al.* 2004b; Bao *et al.* 2009; Li *et al.* 2010; Zhang *et al.* 2013). The original work by Wang & Su (1987) reported six breccia pipes based on negative topography and identified the pipes as having two phases: vent and crater. On the basis of abundant pyroxenite xenoliths and clinopyroxene xenocrysts in the breccia, Li *et al.* (2001) interpreted the brecciated pipes as mica-olivine pyroxenite. Li *et al.* (2001) believed that the pyroxenite and clinopyroxene came from the nearby layered intrusion, and therefore suggested that the breccia pipes formed after the solidification of the layered intrusion.

Jiang *et al.* (2004b) reported the major and trace element compositions of 7 breccia clasts and 6 matrix samples from the breccia pipes. They interpreted the breccia and matrix compositions to be similar, and the samples to be homogeneous, based on selected trace element patterns. They considered a matrix sample with MgO = 18.78 % to represent a primary magma composition. Jiang *et al.* (2004b) also recognized dykes and other intrusions in the area, which they inferred to be related to the breccia pipes, and described chlorite and serpentine alteration in the breccia.

Bao *et al.* (2009) used REE and trace element to classify the breccia as kimberlitic brecciated peridotite, based on trace element patterns. They noted there were differences from typical kimberlites in major oxide composition, higher HREE concentrations, and the absence of indicator minerals such as high-Cr chromite, pyrope and magneso-ilmenite. In contrast, Li *et al.* (2010) reported whole rock major and trace element results on five samples analyzed in bulk as well as analyses of separated breccia clasts and matrix. Their reported SiO_2 contents in breccia and matrix phases were 41.86 % and 31.25 %, respectively, which were higher than their reported whole rock data (average = 30.10 %). They classified the breccia as picritic in composition.

While the pyroxenite xenoliths are postulated to come from the Wajilitag layered intrusion, no geochemical or field relationships have been observed to confirm this. No relative age relationships can be confirmed between the breccia pipes, associated dykes and Wajilitag layered intrusion. While some chemical features suggest the breccia pipes are similar to kimberlites in composition, pervasive alteration of breccia makes conclusive classification challenging. Associated dykes appear less altered, and may provide more robust geochemical data. The dykes also have significantly less heterogeneity than is seen in kimberlite pipes (Le Maitre 2002; Patterson *et al.* 2009; and references therein).

Bachu breccia pipe geochronology

Li *et al.* (2001) reported an ^{40}Ar-^{39}Ar age of phlogopite in a breccia pipe as 252.7 Ma. Zhang *et al.* (2013) reported a single-crystal perovskite U-Pb age on a breccia pipe with 23 grains as 299.8 ± 4.3Ma (2σ) and two single-crystal baddeleyite U-Pb ages on 2 samples with 21 spots each from the same dyke as 300.8 ± 4.7 Ma (2σ) and 300.5 ± 4.4 Ma (2σ). For perovskite dating, Zhang *et al.* (2013) analyzed bulk breccia that was powdered after visible xenoliths had been manually removed. Bao *et al.* (2009) and Li *et al.* (2010) noted that it would be difficult to remove all xenoliths in this way.

The age span of perovskite ages is 30.6 Ma, from 284.2 to 314.8 Ma (Fig. 9a). These ages do not overlap within analytical error (Fig. 9a). Perovskites appear heterogeneous, with Th concentrations ranging from ~400 to ~6300 ppm. Heterogeneity in perovskite has been observed in the Elliot County kimberlite, where multiple perovskite populations differ in size, morphology and composition, and have Th concentrations ranging from 43 to 1726 ppm, and the $^{206}Pb/^{238}U$ ages vary from 79.4 to 102.8 Ma (Heaman 1989). Additional studies have shown perovskite morphology, composition and age can be very complicated in kimberlites (e.g. Heaman & Kjarsgaard 2000; Sarkar *et al.* 2011). Bachu perovskite morphology and composition appear quite complex (Bao *et al.* 2009; Zhang *et al.* 2013), and therefore the large observed age range may be attributed to heterogeneity in perovskite populations. While the Bachu dykes have been inferred to be the same age as Bachu breccia (Zhang *et al.* 2013), other kimberlite localities such as Buffonta (Kirkland Lake fields, Canada) show breccia and dykes that are recognizably different in age (breccia: 146 Ma, dykes: 153 Ma, Heaman & Kjarsgaard 2000). Moreover, the analytical error (1σ) of $^{207}Pb/^{235}U$ ratio of perovskite dating in Zhang *et al.* (2013) is remarkably large, with an average of 42 % and up to 94 %, which is more than an order of magnitude higher than corresponding errors of $^{207}Pb/^{206}Pb$ and $^{206}Pb/^{238}U$ ratio. Without additional information on the experiment, it is hard to access the source of the large error of $^{207}Pb/^{235}U$ ratio. This also affects the reliability of this data.

The baddeleyite U-Pb ages also show a large range within each sample, from 278.2 to 328.6 Ma for DW21-1 and 272.6 to 321.2 Ma for DW21-4 in Zhang *et al.* (2013). For both samples, more than half of individual spot ages do not overlap each other within error (Fig. 9b and 9c). Weighted mean average data for DW21-1 show five distinctive age groups, with weighted mean ages of each group at 278.2 ± 7.6 Ma, 288.5 ± 7.2 Ma, 301.5 ± 6.1 Ma, 310.5 ± 7.6 Ma and 326 ± 10 Ma (Fig. 9c). This suggests that baddeleyite populations are heterogeneous, and the age clusters may represent several episodes of crystallization, occurring at 10 to 16 Myr intervals. The Th concentration for baddeleyites varies dramatically, from 1 to 40 ppm for DW21-1 and from 2 to 221 ppm for DW21-4. Such big age spans and chemical variation are outside analytical error (~5% for SIMS dating). Instead, it could be linked to magma mixing of multiple pulses. Further investigation of geochronological work on the Bachu breccia and dykes is required to address this.

Bachu breccia geochemistry

It is difficult to obtain reliable geochemical signatures of primary, unaltered kimberlite due to the combined effects of crustal assimilation and element mobility during post-emplacement alteration processes (e.g. Mitchell 2008; Donatti-Filho *et al.* 2013; Sarkar *et al.* 2014). Researchers usually use fresh hypabyssal kimberlite to try to minimize the effects of contamination and secondary alteration (e.g. Le Roex *et al.* 2003;

Harris *et al.* 2004; Becker & Le Roex, 2006). However, the published geochemistry data of Tarim are all from surface samples of brecciated material (Jiang *et al.* 2004b; Bao *et al.* 2009; Li *et al.* 2010) which has been altered (Li *et al.* 2001; Jiang *et al.* 2004b; Bao *et al.* 2009). This makes it complicated to identify geochemical signatures of primary magma compositions.

Recently, Beyer *et al.* (2013) reported a relatively large set of partition coefficient (D) values of incompatible elements (15 elements) between perovskite and kimberlite melt at 1.5 GPa and 1200 ℃. Sarkar *et al.* (2014) suggested that the perovskite composition and D value could be used to calculate liquid compositions in equilibrium with measured perovskite minerals, in an effort to quantify the original uncontaminated magma composition. Following this approach, we use a suite of trace element concentrations of perovskite measured in previous works to calculate the magma composition in equilibrium with those perovskites (Nb, La, Ce, Pr, Nd, Sm, Eu and Gd, Table 7). Calculated melt compositions from perovskite data systemically shows an order of magnitude higher concentrations than those measured from the breccia pipe data (Fig. 9d, see figure caption for detail). This suggests that perovskites are not in equilibrium with the host matrix composition. Furthermore, the large-ion lithophile element concentrations (LILE, e.g. K, Rb and Ba) vary dramatically among different samples, by 300%, 2300% and 580%, respectively. REE concentrations are quite uniform and incompatible element pairs such as La/Sm and Zr/Nb only vary by 90% and 64%, respectively. These indicate that the REE are not as affected by alteration as the LILE, and REE may be more robust in estimate the pre-alteration condition of Bachu pipes.

In summary, the large diversity of Th concentrations and large age span among single grains of both perovskite and baddeleyite, together with the large analytical error of $^{207}Pb/^{235}U$ ratio of perovskite, and age clusters of baddeleyite, make the dating complex. The disequilibrium between perovskite and kimberlite further hinders a proper interpretation of the dating. All the evidences indicates magma mixing of multiple pulses, which have been widely recognized in other kimberlite fields (e.g. Gibeon kimberlite, Namibia, Davies *et al*. 2001; Sparks 2013), which is inconsistent with the idea that these kimberlites were emplaced as a single magmatic event.

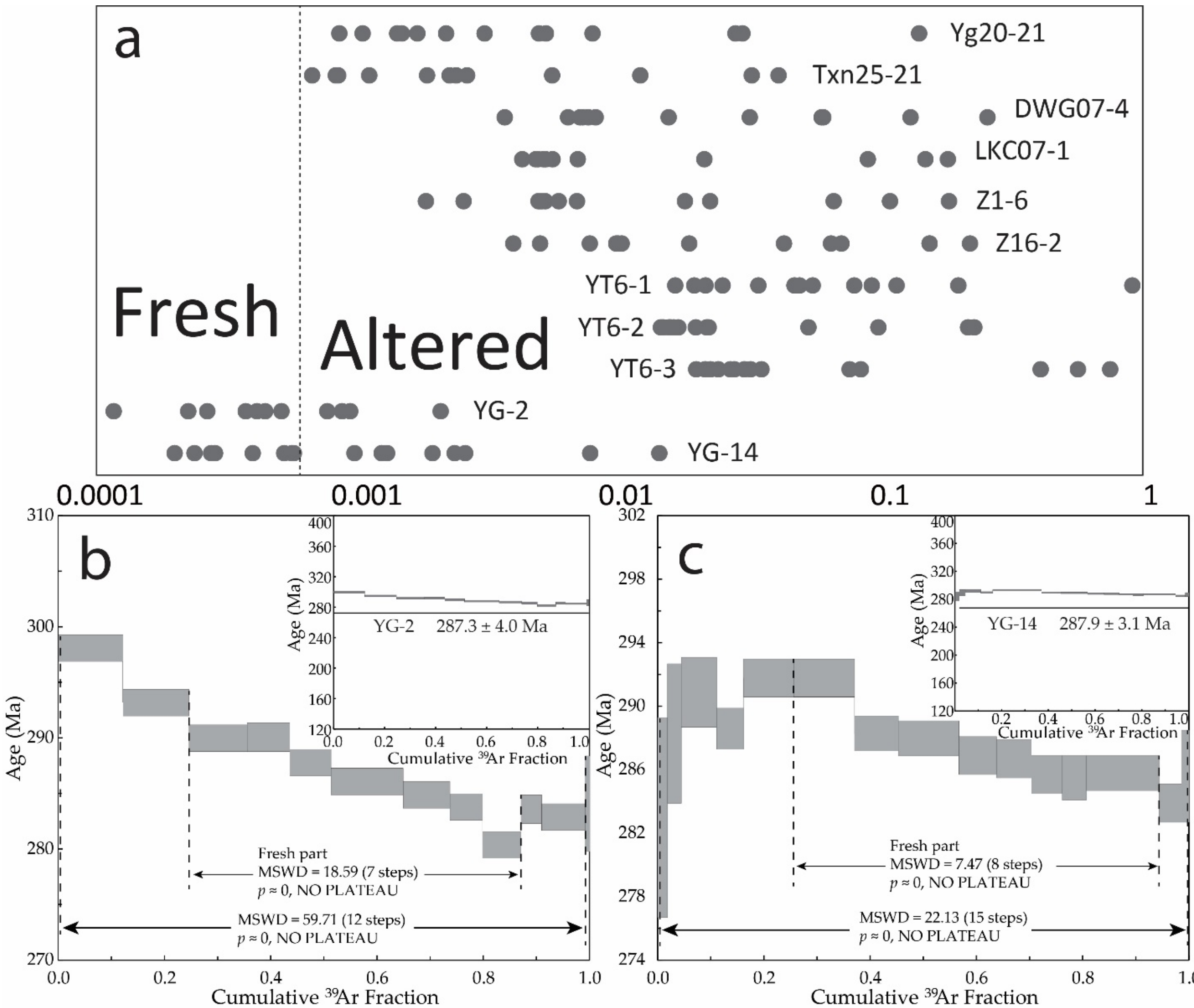

Fig. 1. (a), Assessing the alteration state (A.I.) of 11 basaltic samples for plateau ages. The plot on a log scale is normalized to J = 0.010, and K = 0.65% (see Baksi 2007a, b for details). The cutoff for freshness is shown by the dashed line at A.I. = 0.00060. Sample Yg20-21, Txn25-21, DWG07-4, LKC07-1, Z1-6, Z16-2, YT6-1, YT6-2, YT6-3 are totally altered. Only some steps in YG-2 and YG-14 fall into fresh zone. Yg20-21 and Txn25-21 from Yang *et al.* (2006); DWG07-4, LKC07-1, Z1-6 and Z16-2 from Zhang *et al.* (2010); YT6-1, YT6-2 and YT6-3 from Liu *et al.* (2012); YG-2 and YG-14 from Wei *et al.* (2014). A.I. are plotted on a log scale. After Fig. 2 of Baksi (2012). (b) and (c), $^{40}Ar/^{39}Ar$ plateau age spectra for YG-2 and YG-14 from Wei *et al.* (2014). The small figures in right corners are

the original scale spectra (120 Ma to 400 Ma), which can give visually acceptable plateaus. The redrawn plateau age spectra show clear “bumps” and no plateau. Fresh parts stand for the steps that pass the A.I. test (A.I. < 0.0006).

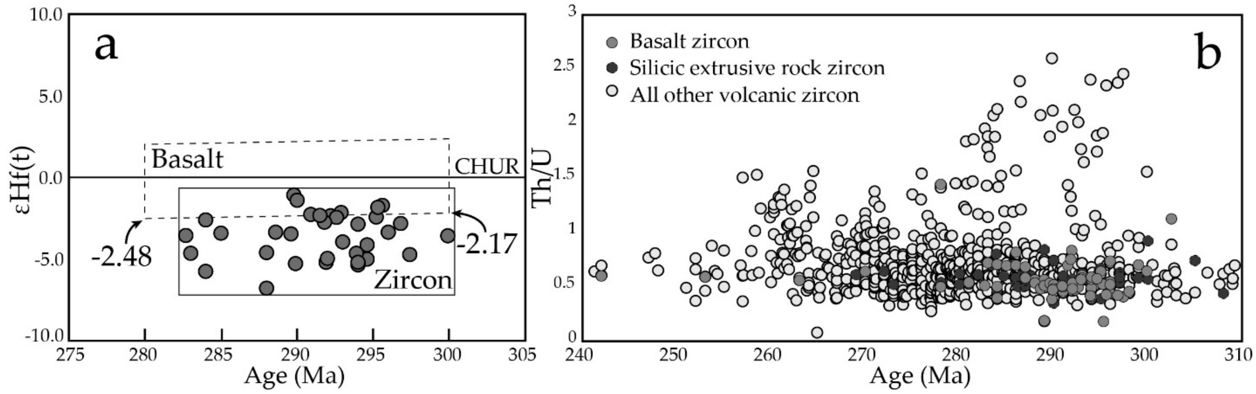

Fig. 2. (a), Zircon Hf isotopic features of basalt zircon and host basalt. Basalt zircon Hf isotopic data from Zhang *et al.* (2010b, 2012) and Li (2013). Basalt Hf isotopic data from Li (2013). The εHf(t) of each zircon grain is recalculated to corresponding single grain age, using $^{176}Lu/^{177}Hf_{CHUR}$=0.0036, $^{176}Hf/^{177}Hf_{CHUR}$=0.282785 (Bouvier *et al.*, 2008). Solid frame shows the area of Keping zircon εHf(t), the dashed frame shows the basalt εHf(t) range recalculated from 300 to 280 Ma. (b), Single grain age vs Th/U ratio of zircons. The Xiaotiekanlike silicic extrusive rock zircons from Luo *et al.* (2013) and Liu *et al.* (2014). The Keping basalt zircons from Li *et al.* (2007), Zhang *et al.* (2009), Yu (2011) and Zhang *et al.* (2012). All other volcanic zircon are extracted from 48 published data. We use the age range of 310 to 240 Ma, and sporadic older ages are not shown. The basalt zircon, silicic extrusive rock zircon and all other volcanic zircon are completely overlap with each other. Then the Th/U ratio cannot be a criteria for discrimination.

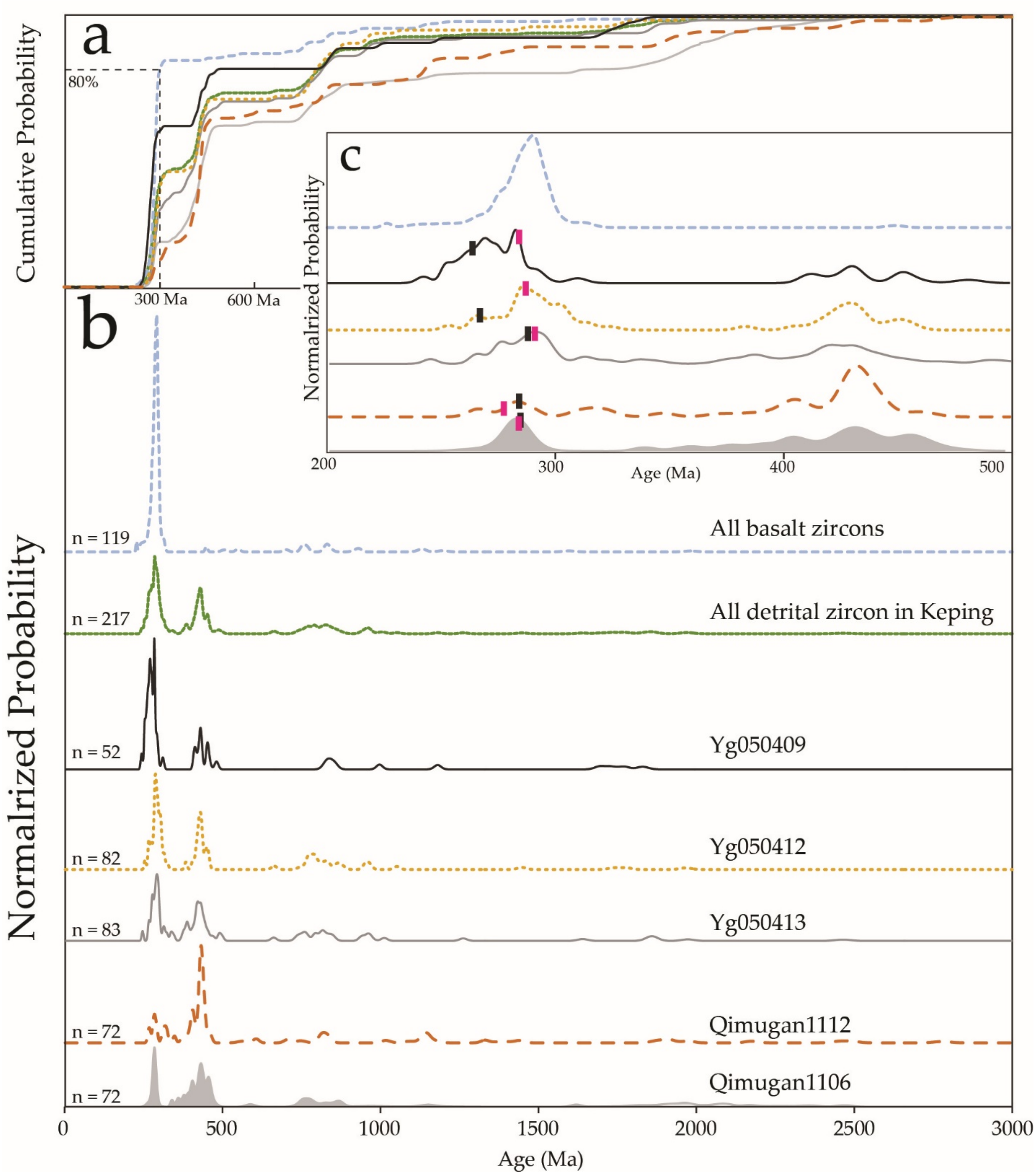

Fig. 3. (a), Cumulative probability plots show graphic distribution among all basalt zircons, all Keping detrital zircons, three single layers of Keping sandstone and two single layers of Qimugan sandstone. The dashed line demonstrates strong signature of < 300 Ma population of basalt zircon, which is significantly different from any other

detrital zircon pattern. See basalt zircon section for detail. (b), Diagram showing the distribution of basalt zircon ages and detrital zircon ages. Each curve is constructed by summing all of the concordant individual ages and uncertainties and then normalizing by the number of analyses (shown on the left) such that each curve contains the same area. Calculated $^{206}Pb/^{238}U$ ages were used for zircons younger than 1 Ga, whereas the $^{206}Pb/^{207}Pb$ ages were reported for older zircons (Gehrels *et al.*, 2008; Gehrels 2012). (c), Detail of Figure B, with 200 to 500 Ma grains. A more monotonous basalt zircon age pattern can be seen, further rule out the possibility of sediments source. The black bars marked on the curve show the YC2σ(3+) of each sample. The pink bars marked the "weighted mean average age of youngest population" in Zou *et al.* (2013) and Li *et al.* (2013). Diagrams are constructed with programs from the Arizona LaserChron Center Web site (http://www.laserchron.org).

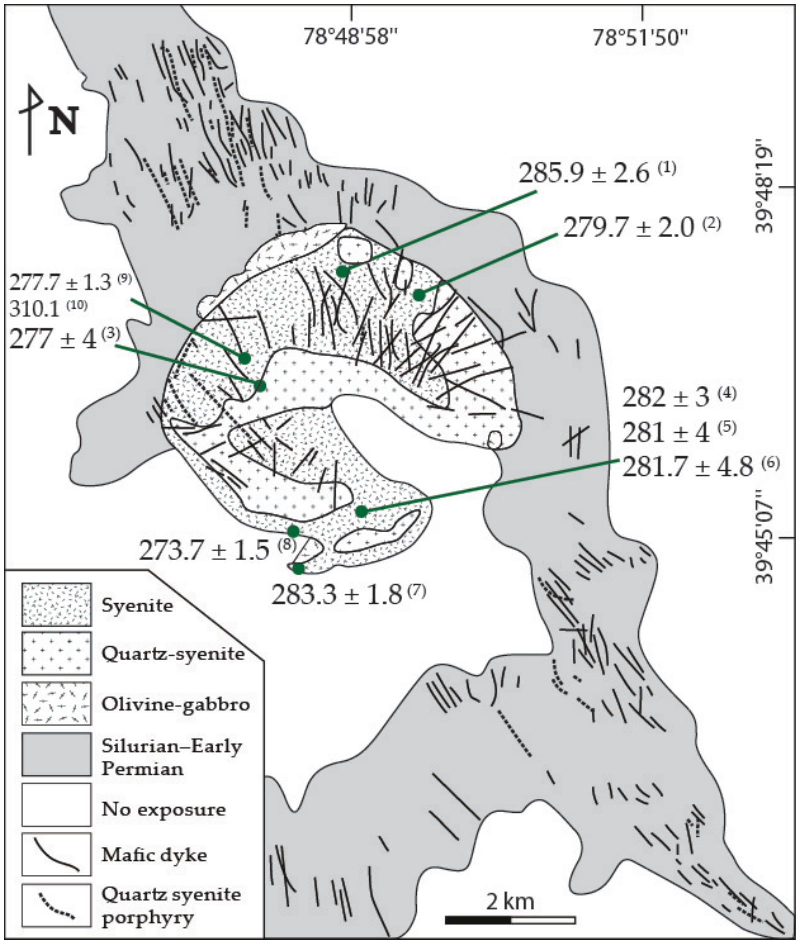

Fig. 4. Detailed geological map of the mafic and felsic dykes around the Xiaohaizi syenite intrusion (Modified after Zhang *et al.* 2008b and Wei & Xu 2011). (1) - Sun *et al.* (2008), (2) - Wei & Xu (2011), (3) -Yang *et al.* (2006), (4) and (5) - Li *et al.* (2007), (6) - Zhang *et al.* (2009), (7) - Sun *et al.* (2009), (8) - Zhang *et al.* (2008a), (9) -Yang *et al.* (1996), (10) - Liu *et al.* (2004). Data (8) is marked as the GPS coordinate in Zhang *et al.* (2008a). Data (1), (3) and (7) are noted as marked in the original source figures. Data (2), (4), (5), (6), (9) and (10) are marked as inferred position from the statement of original sources.

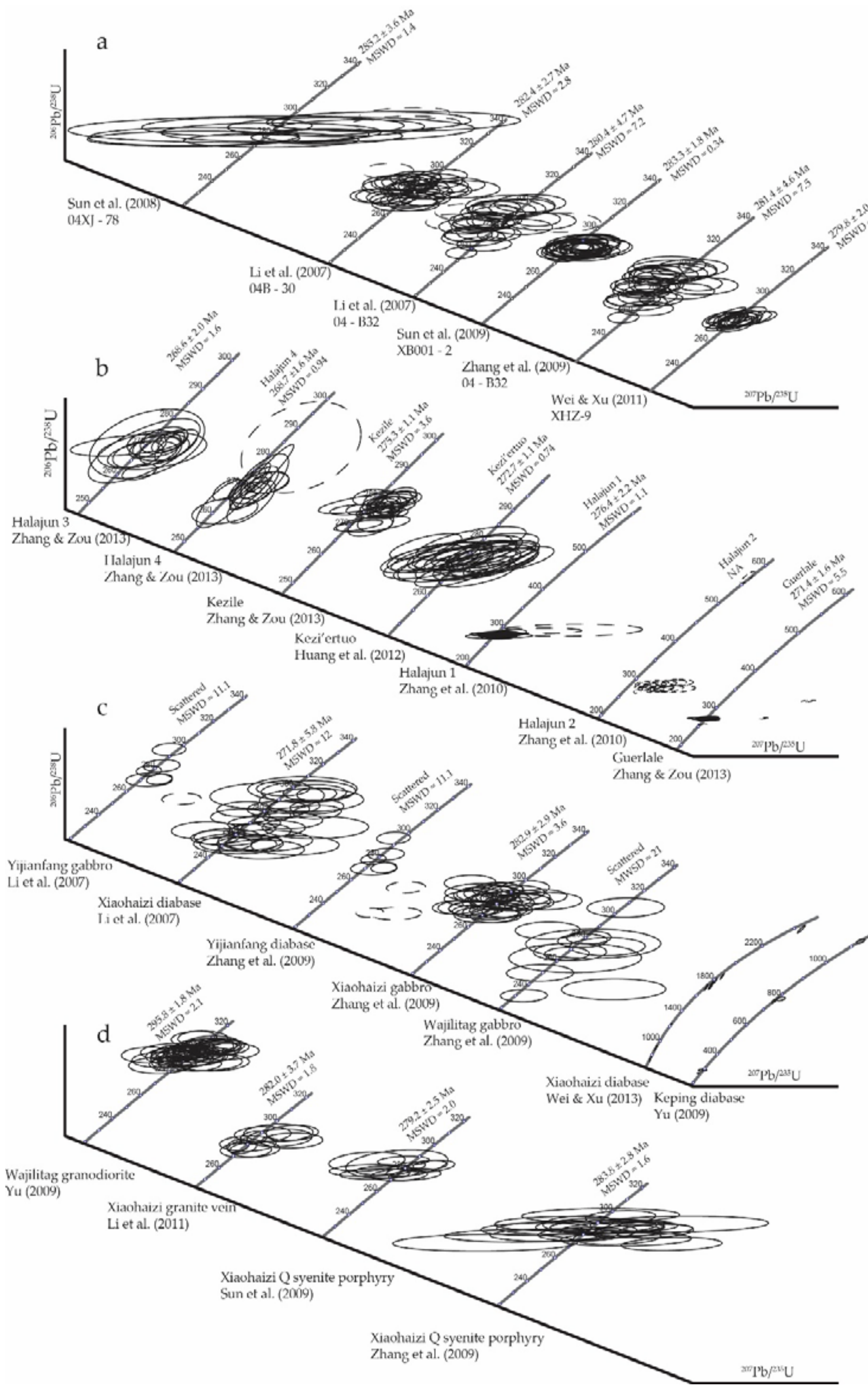

Fig. 5. (a), U-Pb concordia plot of zircon ages from published data of Xiaohaizi syenite intrusion. The solid circles show concordant data points, which are used for weighed mean average age recalculation (shown on top of each concordia line), and dashed

circle show the data points eliminated (see text for detail). Uncertainties are shown at the 1σ level. Diagram was constructed with the use of Isoplot version 3.6 (Ludwig 2008). The sample BC03 from Zhang *et al.* (2008) has uniformly negative RHO, and is not plotted. The sample XH-13 from Yang *et al.* (2006) does not have $^{207}Pb/^{235}U$ ratio raw data, and is not plotted. (b), U-Pb concordia plot of ages of zircon from published data of seven granite plutons in the Halajun area. The solid circles show the concordant data points, which are used for weighed mean average recalculation (shown on top of each concordia line), and dashed circles show the data points eliminated (see text for detail). Uncertainties are shown at the 1σ level. Data points of 6, 8, 12, 15 of Halajun 3 and point 18 of Halajun 4 are not shown because they are out of figure range. Note the difference in scale of the concordance lines. (c), U-Pb concordia plot of ages of zircon from mafic dikes in Tarim. The solid circles show the concordant data points, which are used for weighed mean average age recalculation (shown on top of each concordia line), and dashed circles show the data points eliminated (see text for detail). (d), U-Pb concordia plots of ages of zircon from silicic dikes in Tarim. The solid circles show the concordant data points, which are used for weighed mean average age recalculation (shown on top of each concordia line).

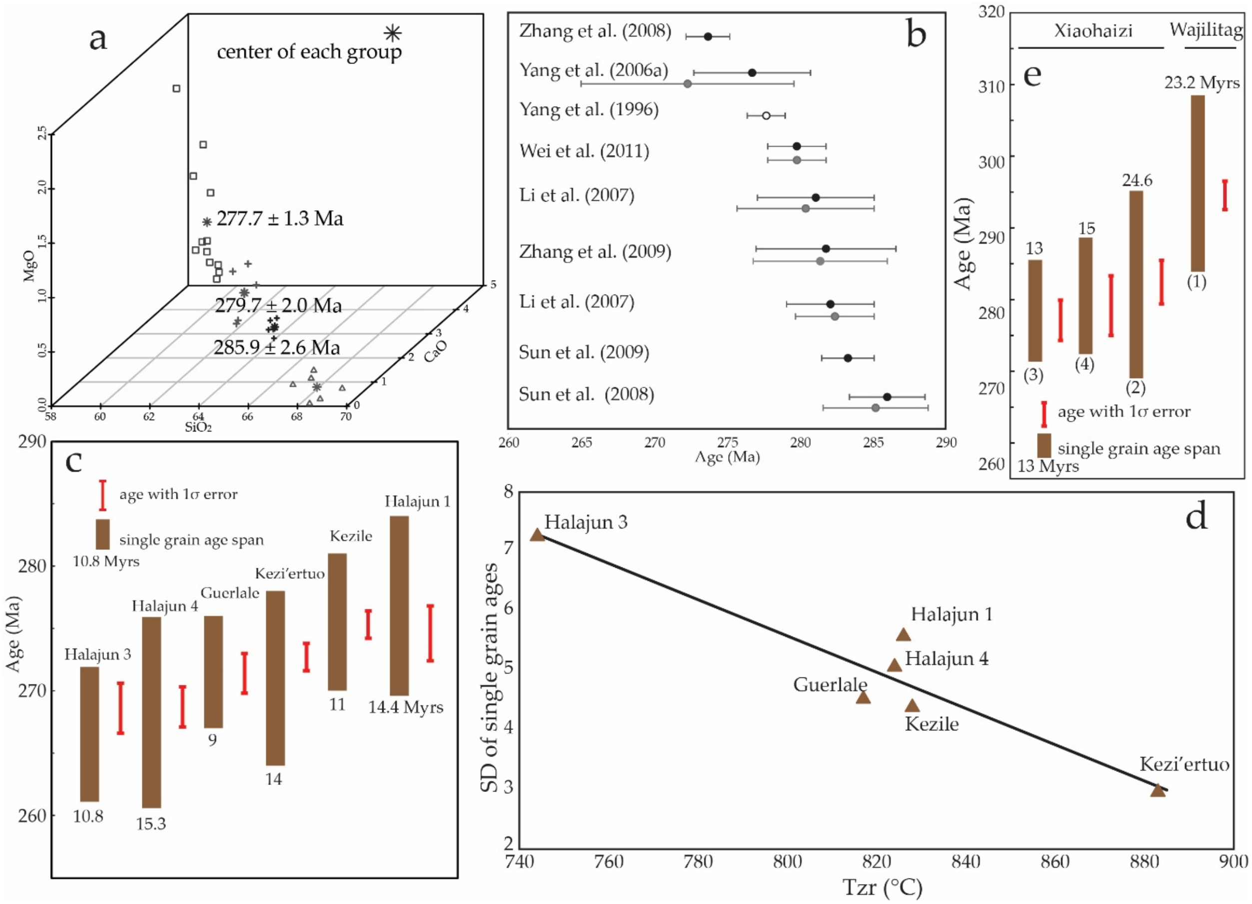

Fig. 6. (a), SiO_2 vs. MgO vs. CaO three-dimensional diagram of Xiaohaizi syenite intrusion, with corresponding ages marked. The published major element geochemistry data can be clustered into four groups by using K-means approach (Stuart 1982), with the clustering center of each group having SiO_2 content of 60.98%, 63.53%, 65.29% and 68.12% respectively. For syenite geochemistry data, see Supplementary material 4. Diagram was constructed with the use of R project version 3.1.0 (R Development Core Team 2008). (b), Age distribution of published data of Xiaohaizi syenite intrusion and the results of recalculation. Black solid dot and bar shows the data derived by zircon U-Pb method, black hollow dot and bar shows the data derived by whole rock $^{40}Ar/^{39}Ar$ method, and the grey solid dot and bar shows the result after recalculation. (c), The age distribution after recalculation, and single grain ages. Still, big spans occur within each sample, indicating complex magmatism. (d), The Zr saturation temperature (T_{zr}) vs.

standard deviation of single grain ages of individual sample. The zircon saturation temperature is calculated using the empirical equation by Watson & Harrison (1983). $T_{Zr} = 12{,}900 / [2.95 + 0.85M + \ln(496{,}000 / Zr_{melt})]$, whereas M = [(Na + K + 2·Ca)/(Al·Si), all in cation fraction]. A negative correlation can be observed, with the fitting curve standard deviation = -0.0303 T_{zr} + 29.854. The granite geochemistry data used to calculate T_{zr} are summarized in Supplementary material 4. (e), the age distribution of silicic dikes after recalculation, and single grain ages after eliminating of discordant data points and obvious xenocrysts. (1) - Yu (2009); (2) - Li *et al.* (2011); (3) - Sun *et al.* (2009); (4) - Zhang *et al.* (2009).

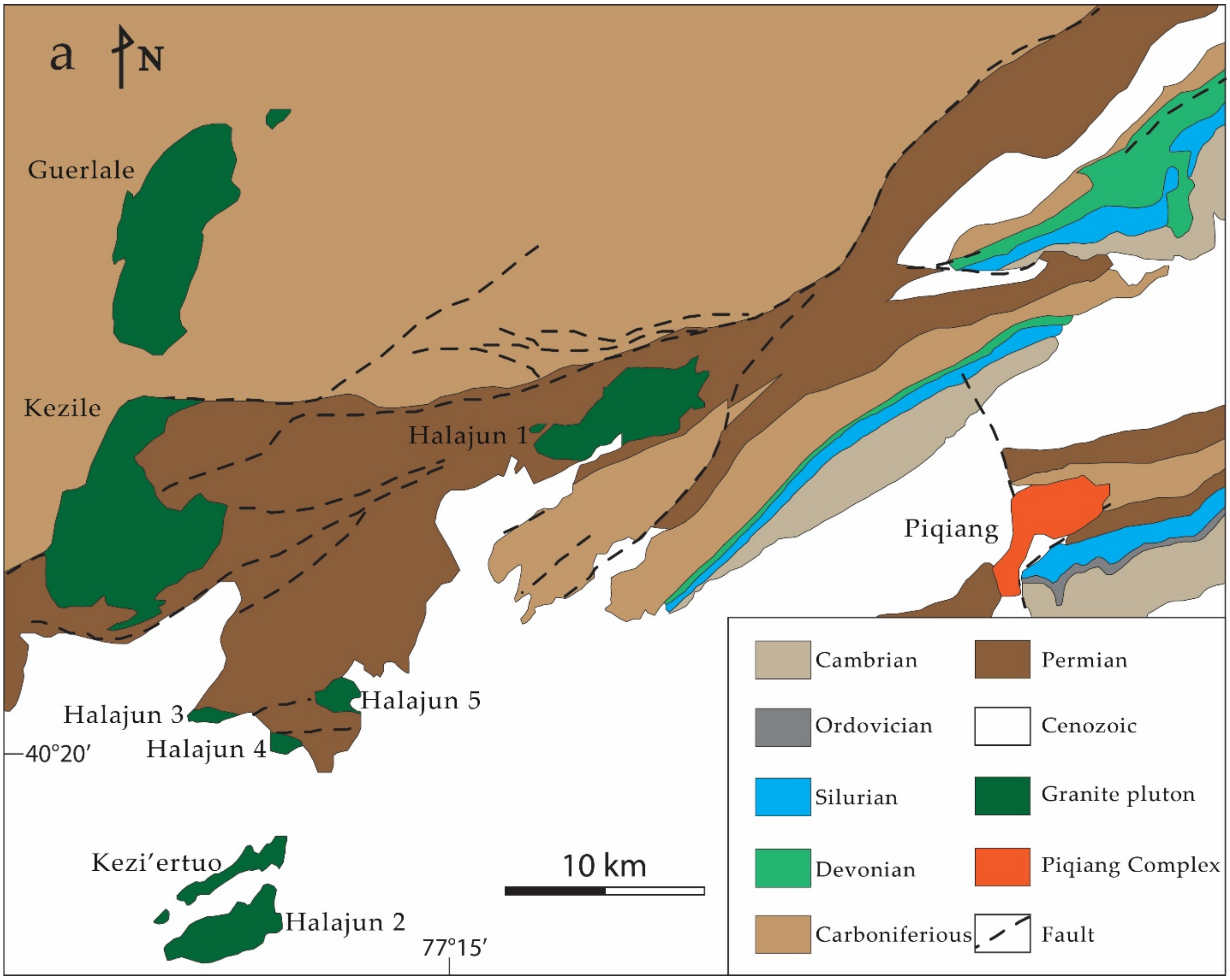

Fig. 7. Geological map of the Halajun region. Modified from Huang *et al.* (2012) and Zhang & Zou (2013). Note that Kezi'ertuo pluton is wrongly marked as "HEK" in Huang *et al.* (2012) (Huang pers. comm. 2014), and Kezi'ertuo pluton is taken as a part of Halajun 2 pluton in Zhang & Zou (2013).

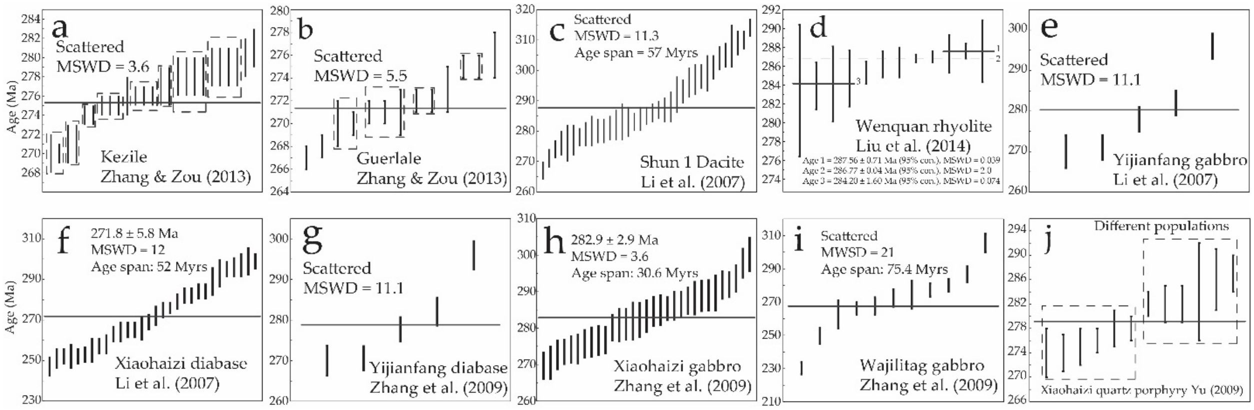

Fig. 8. (a), Weighed mean average plot of Kezile pluton with ages chronologically arranged. The dashed frames show the visually distinctive age populations. (b), Weighed mean average plot of Guerlale pluton with ages chronologically arranged. The dashed boxes show the visually distinctive age populations. (c), the weighted mean average plot of Shun1 and Shun1 from Li *et al.* (2007) and Zhang *et al.* (2011), after eliminating discordant data points and obvious xenocrysts. (d), The weighted mean average plot of WQ09-2 rhyolite from Liu *et al.* (2014). The youngest four analysis and oldest three analysis constitute two distinct groups, with weighted mean average ages of 287.56 ± 0.71 Ma (95% conf., MSWD = 0.039) and 284.20 ± 1.60 Ma (95% conf., MSWD = 0.074) respectively. (e), (f), (g), (h) and (i), Weighed mean average plot of mafic dykes. All of the dates have either highly scattered or big age span of single grain ages. (j), Weighed mean average plot of Xiaohaizi quartz syenite porphyry from Yu (2009). The dashed frames show the visually distinctive age populations. The single grain ages of all these dating are discrete, and therefore their weighed mean average ages are equivocal.

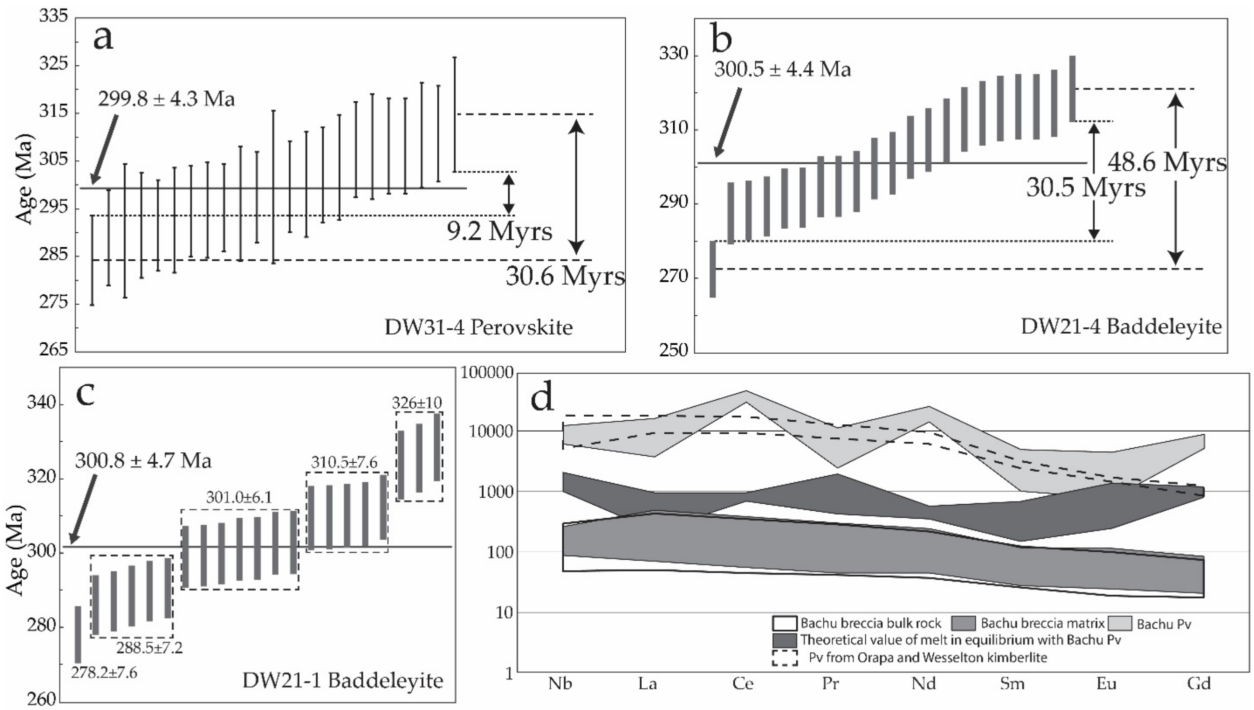

Fig. 4. (a), Weighted mean average plot of DW31-4 perovskite from Zhang *et al.* (2013). The perovskites have a big age span of 30.6 Ma, and the oldest and youngest perovskites do not overlap within 1σ error, with a gap of 9.2 Ma. (b), Weighted mean average plot of DW21-4 baddeleyite from Zhang *et al.* (2013). The baddeleyites have a big age span of 48.6 Ma, and the oldest and youngest perovskites do not overlap within 1σ error, with a gap of 30.5 Ma. (c), Weighted mean average plot of DW21-1 baddeleyite from Zhang *et al.* (2013). At least five age groups can be recognized, with weighted mean ages of each group at 278.2 ± 7.6, 288.5 ± 7.2, 301.5 ± 6.1, 310.5 ± 7.6 and 326 ± 10 Ma (shown by the dashed frames). (d), Primitive mantle-normalized selected REE plot of Bachu perovskite (Pv), Bachu breccia (bulk rock and matrix), theoretical melt calculated by partition coefficients (D) and Pv in Sarkar *et al.* (2011). Primitive mantle values after Sun & McDonough (1989). REE value of Bachu Pv is from Zhang *et al.* (2013), and was carried out by electron microprobe. The serrate normalized REE pattern is probably due to experimental error, by which the low abundance elements are affected (e.g. Pr, Sm and Gd). Bachu breccia bulk rock REE value is from Bao *et al.* (2009).

Bachu breccia matrix REE value is from Jiang *et al.* (2004) and Li *et al.* (2010). Theoretical value of melt in equilibrium with Bachu Pv is calculated using partition coefficients (D) from Beyer *et al.* (2013) and Melluso *et al.* (2008) (for the elements with no D available in Beyer *et al.* (2013)). Primitive mantle-normalized REE value of Pv in Sarkar *et al.* (2011) is shown for reference, which are from twelve Orapa and one Wesselton kimberlite samples in Botswana and South Africa respectively. Notice that the theoretical value of melt in equilibrium with Bachu Pv is one magnitude higher than both Bachu breccia bulk rock and matrix. For kimberlite geochemistry data, see Supplementary material 4.

Table 1. *Assessment of the validity of the published whole rock ^{40}Ar-^{39}Ar ages.*

Unit	Sample number	Rock type	Plateau age(Ma)	Statistics	Alteration state (K %)	Validity of age based on statistics/freshness
3/4 KP	Yg20-21	Basalt	281.8±4.2	F=0.21(3) p~0.81	Altered （1.20）a	Rejected-altered, no plateau (3 steps, 35.82%)
Damusi	Txn25-21	Basalt	290.1±3.5	F=82.68(7) p~0	Altered （1.20）b	Rejected-altered, no plateau
Fang 1	Fang1-10	Diabase	330.7±26.0 d	F=343.60(9) p~0		Rejected-no plateau
Keping	DWG07-1	Diabase	274.08±2.35	F=1.59(4) p~0.19		Rejected-no plateau (4 steps, 42.34%)
Keping	DWG07-4	Basalt	271.93±3.67	F=10.08(6) p~0	Altered （0.72）	Rejected-altered, no plateau
Keping	LKC07-1	Basalt	282.90±1.55	F=1.16(6) p~0.33	Altered （1.21）	Rejected-altered
Tangwangcheng	TWC07-1	Diabase	262.30±4.05	F=7.59(7) p~0		Rejected-no plateau
Xiaohaizi	XHZ07-7	Diabase	285.38±8.47	F=53.80(7) p~0		Rejected-no plateau
Zhong 1	Z1-6	Basalt	268.88±4.15	F=18.48(5) p~0	Altered （1.01）	Rejected-altered, no plateau
Zhong 16	Z16-2	Basalt	271.05±3.47	F=7.32(4) p~0	Altered （1.14）	Rejected-altered, no plateau
Yangta 6	YT6-1	Basalt	261.1±4.89	F=3.72(3) p~0.02	Altered （1.58）	Rejected-altered, no plateau
Yangta 6	YT6-2	Basalt	252.32±3.47	F=6.68(10) p~0	Altered （1.43）	Rejected-altered, no plateau
Yangta 6	YT6-3	Basalt	367.44±3.01	F=5.96(10) p~0	Altered （1.62）	Rejected-altered, no plateau
Yingmai 16	YM16-3	Rhyolite	266.92±1.73	F=1.92(9) p~0.05		Rejected-no plateau
Yudong 2	YD2-2	Metamorphic diabase	248.84±4.75	F=19.20(12) p~0		Rejected-no plateau
Keping	YG-2	Basalt	287.3±4.0	F=59.71(12) p~0	Altered （1.22）	Rejected-altered, no plateau
Keping	YG-14	Basalt	287.9±3.1	F=22.13(15) p~0	Altered （1.12）	Rejected-altered, no plateau
Keping	KP-4	Basalt	277.54±0.72 e	F=5.28(4) p~0	c	Rejected-altered, no plateau
Xiaohaizi	XH-8	Syenite	277.7±1.3	F=0.17 (4) P~0.92		Valid plateau
Piqiang	9-1K	Gabbroid	265.5±1.2 f	F=32.17(8)P~0		Rejected-no plateau

Based on the statistical analysis of age spectra and alteration state of the sites from which the argon was derived. Yg20-21 and Txn25-21 from Yang *et al.* (2006); Fang1-10 from Zhang *et al.* (2009); DWG07-1, DWG07-4, LKC07-1, TWC07-1, XHZ07-7, Z1-6 and Z16-2 from Zhang *et al.* (2010); YT6-1, YT6-2, YT6-3, YM16-3 and YD2-2 from Liu *et al.* (2012); YG-2 and YG-14 from Wei *et al.* (2014); KP-4 from Chen *et al.* (1997b); XH-8 from Yang *et al.* (1996); 9-1k from Zhou *et al.* (2010). Plateau ages listed with 2σ errors. F=MSWD value of plateau section, calculated from MSWD = ∑

$[(t_i-T)^2/(dt_i)^2]/(N-1)$, where $T = \sum[(t_i/(dt_i)^2]/ \sum (dt_i)^{-2}$, t_i and dt_i stand for individual step ages and associated error (1σ). N = number of steps used shown in parentheses. *p* = probability of fit as derived from Chi Square Tables (e.g. DeVor *et al.* 1992). Sample are altered if their alteration index is > 0.00060. K % takes from where $^{40}Ar/^{39}Ar$ dating and major element composition results are reported together. For $^{40}Ar/^{39}Ar$ dating without major element composition results, we take K % from other sources with adjacent sample location. a, From average K % of 14 samples in Wei *et al.* (2014). b, From sample Txn25-21 in Li *et al.* (2008). c. No ^{36}Ar data available to calculate A.I. d. No statement of step ages used and error level, we take 5 to 13 steps and 2σ. e. No statement of step ages used or error level, we take last four steps and 2σ. f. No statement of error level, we take 2σ. After Table 1 of Baksi (2012).

Table 2. *Summary of published data of syenite body and recalculation.*

Age (Ma)	Recal Age (Ma)	MSWD	Spots	Method	mineralogy	Rock name in paper	Author
310.1				**K-Ar**		**amphibole syenite**	**Liu *et al.* 2004**
285.9±2.6	**285.2 ± 3.6**	**1.4**	**15/15/13[c]**	**SHRIMP**	**Afs(Ab+Pth) 70-95%, Pl 13%-15%, Qtz 2%-5%, Hbl minor**	**syenite**	**Sun *et al.* 2008**
283.3±1.8	**283.3±1.8**	**0.34**	**25/25/25**	**LA-ICPMS**	**Pl, Pth, Aug, Ol minor**	**pyroxene syenite**	**Sun *et al.* 2009**
282±3	**282.4 ± 2.7**	**2.8**	**30/29/28**	**LA-ICPMS**		**syenite**	**Li *et al.* 2007**
281.7±4.8	**281.4 ± 4.6**	**7.5**	**27/27/27**	**LA-ICPMS**		**syenite**	**Zhang *et al.* 2009**
281±4	**280.4 ± 4.7**	**7.2**	**33/28/25**	**LA-ICPMS**		**syenite**	**Li *et al.* 2007**
279.7±2	**279.8 ± 2.0**	**0.26**	**18/17/17**	**SIMS**	**Afs(Ab+Pth) 85%, Hbl 4%, Bt 5%, Qtz 2%-4%, Pl 1-2%, minor Ap, Ilm, Zrn**	**amphibole syenite**	**Wei *et al.* 2011**
277.7±1.3[a]				**WR (?) Ar-Ar**	**Afs(Ab+Atc) 70-95%, Pl, Qtz, a little Hbl, occasional Aug, Ol, minor Zrn, Ap, Aln, Ttn**	**syenite**	**Yang *et al.* 1996**
277±4	**272.3 ± 7.3**	**4.0**	**15/? a/15**	**SHRIMP**		**syenite**	**Yang *et al.* 2006a**
273.7±1.5[b]				**LA-ICPMS**	**Afs(Or) 40-70%, Qtz 10-30%, Hbl 5-10%, Bt 1-2%, minor Zrn, Ap, Rt, Aln, Mnz**	**quartz-syenite**	**Zhang *et al.* 2008**

Age recalculation is after eliminating the spots with RHO value out of 0 to 1 or off the concordance curve. RHO value is calculated as RHO = $\{[(^{207}Pb/^{235}U)_{ERROR}/(^{207}Pb/^{235}U)_{RATIO}]^2+[(^{206}Pb/^{238}U)_{ERROR}/(^{206}Pb/^{238}U)_{RATIO}]^2-[(^{207}Pb/^{206}U)_{ERROR}/(^{207}Pb/^{206}U)_{RATIO}]^2\}/\{2\times[(^{207}Pb/^{235}U)_{ERROR}/(^{207}Pb/^{235}U)_{RATIO}]/\ [(^{206}Pb/^{238}U)_{ERROR}/(^{206}Pb/^{238}U)_{RATIO}]\}$ (Schmitz & Schoene 2007). The "recal age" is recalculated weighted mean average age. Calculation is conducted by "Isoplot 4.15". Spots column is shown as number of spots dated / after RHO discriminant / after concordance discriminant.

a, See ^{40}Ar-^{39}Ar section for detail. b, All negative RHO values. c, Shown as all the spots/ spots originally used/ spots used here.

Table 3. *Summary of published data of granite plutons and recalculation.*

Location	Age (Ma)	Recal Age (Ma, 2σ)	MSWD	Method	Data points deleted		Points used	Age span	Tzr	STD	Author
					RHO out of 0 - 1	Away from Concordant line					
Halajun 1	278 ± 3	274.6 ± 2.2	1.1	SHRIMP	None	1.1, 1.3	14/13/12	14.4	828	5.59	Zhang *et al.* (2010)
Halajun 2	278 ± 3	a	NA	SHRIMP	None	All	17/16/0	NA	804	NA	Zhang *et al.* (2010)
Halajun 3	268.6 ± 1.5	268.6 ± 2.0	1.6	LA-ICPMS	9	6, 8, 12, 15	20/15/15	10.8	766	7.27	Zhang *et al.* (2013)
Halajun 4	286.8 ± 1.7	268.7 ± 1.6	0.94	LA-ICPMS	5, 6, 13	17	20/15/16	15.3	822	5.08	Zhang *et al.* (2013)
Halajun 5	271 ± 2.2	b	NA	LA-ICPMS	All	None	15/9/0	NA	818	NA	Zhang *et al.* (2013)
Kezile	268.8 ± 1.7	275.3 ± 1.1	3.6	LA-ICPMS	None	None	25/ ? /25	11	824	4.4	Zhang *et al.* (2013)
Guerlale	272.4 ± 1.1	271.4 ± 1.6	5.5	LA-ICPMS	2, 10, 13	3, 15, 16c	21/ ? /15	9	820	4.54	Zhang *et al.* (2013)
Kezi'ertuo	272.7 ± 1.1	272.7 ± 1.1	0.74	LA-ICPMS	None	None	35/35/35	14	883	2.98	Huang *et al.* (2012)

a, Halajun 2 is not recalculated because all of the data points are off the Concordia line, with an exceptional point having an age of 569.1 Ma.

b, Halajun 5 is not recalculated because all data points have negative RHO value.

c, Data point 16 in Guerlale is away from the main cluster and does not overlap with any other data point within error.

d, Zhang *et al.* (2013) mixed up the Concordia plots and raw data between Kezile and Guerlale pluton in the published paper. We assume the raw data to be correct.

Table 4. *Summary of published data of silicic extrusive rocks and comments.*

Sampling sections	Ages(Ma)	Stratum(Formation)	Lithology	Methods	References	Comments
Yingmai 5	286.6±3.3	5484	Dacite	LA-ICP-MS	Tian *et al.* 2010	robust
S79-3	279.6±3.0	4876.5	Dacite	LA-ICP-MS	Yu *et al.* 2011a	robust
S99	273.7±3.2	5263	Dacite	LA-ICP-MS	Yu *et al.* 2011a	robust
S102-1	281.0±3.0	4908	Dacite	LA-ICP-MS	Yu *et al.* 2011a	robust
S114	276.6±2.7	4649.5	Dacite	LA-ICP-MS	Yu *et al.* 2011a	robust
Shun 1	286±4	3461-3465	Dacite-porphyry	LA-ICP-MS	Li *et al.* 2007	Big span
Shun 1	285±11	3461.1-3463.2	Dacite-porphyry	LA-ICP-MS	Zhang *et al.* 2009	Big span
Nanka 1	277.3±2.5	5207	Rhyolite	LA-ICP-MS	Tian *et al.* 2010	Big span
Mana 1	271.7±2.2	5166	Rhyolite	SHRIMP	Tian *et al.* 2010	robust
Yingmai 16	282.9±2.5	5195	Rhyolite	LA-ICP-MS	Tian *et al.* 2010	robust
Yingmai 30	290.9±4.1	6330	Rhyolite	LA-ICP-MS	Tian *et al.* 2010	robust
Wenquan	286.8 ± 0.5	Wenquan	rhyolite	CA-TIMS	Liu *et al.*, 2014	See text

Table 5. *Summary of published data of mafic-silicic dikes and recalculation.*

Sections	Ages(Ma)	Lithology	Methods	Source	Wall rock	Recalculation
Yijianfang	274±15	Gabbro	LA-ICP-MS	Li *et al.* 2007	Syenite body	5 spots, Scattered
Xiaohaizi	272±6	Diabase	LA-ICP-MS	Li *et al.* 2007	Unknown	271.8 ± 5.8, MSWD=12
Yijianfang	283±1.3	Diabase	LA-ICP-MS	Zhang *et al.* 2009	Unknown	5 spots, Scattered
Xiaohaizi	283.1±3.2	Gabbro	LA-ICP-MS	Zhang *et al.* 2009	Unknown	282.9 ± 2.9, MSWD=3.6
Wajilitag	265±16	Gabbro	LA-ICP-MS	Zhang *et al.* 2009	Unknown	Scattered, MSWD=21
Yingan	NA	Diabase	SHRIMP	Yu 2009	Basalt	6 Spots, 268 to 1133 Ma
Xiaohaizi	NA	Diabase	SIMS	Wei *et al.* 2013	Syenite body	17 Spots, 717 to 2390 Ma
Fang 1	330.7±26.0	Diabase	WR Ar-Ar	Zhang *et al.* 2009	Unknown	No plateau
Dawangou	274.08±2.35	Diabase	WR Ar-Ar	Zhang *et al.* 2010	Silurian carbonates	No plateau
Tangwangcheng	262.30±4.05	Diabase	WR Ar-Ar	Zhang *et al.* 2010	Carbonates of unknown age	No plateau
Xiaohaizi	285.38±8.47	Diabase	WR Ar-Ar	Zhang *et al.* 2010	Carbonates of unknown age	No plateau
Yudong 2	248.84±4.75	Metamorphic diabase	WR Ar-Ar	Liu *et al.* 2012	Carbonates of unknown age	No plateau
Xiaohaizi	281.2±3.7	Potash-feldspar-granite vein	LA-ICP-MS	Sun *et al.* 2009	Syenite body	282.0 ± 3.7, MSWD=1.8
Wajilitag	295.9±2.1	Granodiorite	LA-ICP-MS	Zhang *et al.* 2009	Unknown	295.8 ± 1.8, MSWD=2.1
Xiaohaizi	278.4 ±2.2	Quartz syenitic porphyry	SHRIMP	Yu 2009	Sediments	279.2 ± 2.5, Two groups
Xiaohaizi	273.0±3.7	Quartz syenitic porphyry	SHRIMP	Chen *et al.* 2010	Sediments	UE
Xiaohaizi	284.3±2.8	Quartz syenitic porphyry	SHRIMP	Li *et al.* 2011	Silurian and Devonian strata	284.3 ± 2.8, MSWD=1.05

Table 6. *A compilation of all metrics utilized within the study.*

Sample number	Original age	Source	YSG	YPP	YC1σ(2+)	YC2σ(3+)	Comment
QMG1106	284 ± 4 (9)	Li *et al.* (2013)	284 ± 7	284.5	284.7 ± 3.6 (11)	284.7 ± 3.6 (11)	Y1 & Y2 discordant
QMG1112	278 ± 9 (5)	Li *et al.* (2013)	266 ± 4	283.7	268 ± 5.5 (2)	284.1 ± 4.7 (4)	Y1 & Y2 discordant
Yg050409	284	Zou *et al.* (2013)	244 ± 3	270.7	255.3 ± 2.6 (4)	263.7 ± 3.9 (15)	Y1 not overlap
Yg050412	287	Zou *et al.* (2013)	255 ± 3	267.7	267 ± 3.4 (3)	267 ± 3.4 (3)	
Yg050413	291	Zou *et al.* (2013)	247 ± 3	278.2	267 ± 4.2 (2)	287.6 ± 3.8 (21)	Y1 not overlap
All Zou *et al.* (2013)	NA		244 ± 3	269.2	255.2 ± 2.4 (5)	282.4 ± 3.1 (90)	

Note: Y1 and Y2 refer to the youngest and second youngest single grain

Table 7. Selected trace element composition of kimberlitic melt in equilibrium with Bachu perovskite.

Calculated using partition coefficients (D) from Beyer *et al.* (2013) and Melluso *et al.* (2008) for the elements with no D available in Beyer *et al.* (2013). Bachu breccia bulk rock REE value is from Bao *et al.* (2009) and Bachu breccia matrix REE value from Jiang *et al.* (2004) and Li *et al.* (2010) are also showed.

Element	Kd*	Kd**	DW31-4[a]											W10-95[b]	W10-51[b]	W10-11[b]	W10-12[b]	W10-22[b]	W10-52[b]	wjl5-7b[c]	BC701-1[d]	BC702-1[d]	BC702-2[d]	BC701-3[d]
			Theoretical value of melt											Matrix							Bulk rock			
Nb	8.4	16.8	1058	967	700	908	867	875	1075	975	892	1025	1483	61	102	149	179	143	157	124	203	202	186	33
La	25	22.3	496	187	201	150	510	656	173	592	483	323	388	47	130	306	329	204	187	212	288	287	264	33
Ce	26	27.4	1471	1563	1504	1537	1631	1703	1625	1223	1461	1324	1576	96	257	602	668	441	356	449	603	602	555	76
Pr	21	31.3	215	538	348	194	312	279	344	376	291	348	117	12	34	71	81	57	53	59	76	76	70	11
Nd		31.9	614	776	596	606	625	647	647	472	660	596	641	59	139	283	321	190	208	229	285	285	268	48
Sm	16	23	81	81	81	65	199	97	215	301	215	86	156	12	29	49	45	30	31	40	53	54	50	11
Eu		19.8	0	82	0	0	0	55	109	41	232	55	0	4	9	18	19	11	12	11	16	15	14	3
Gd	11	17.3	649	759	475	459	585	554	664	601	712	475	807	12	28	49	39	32	32	32	42	42	39	10

Note: Kd* is from Beyer *et al.* (2013), Kd** is from Melluso *et al.* (2008), a is from Zhang *et al.* (2013), b is from Jiang *et al.* (2004), c is from Li *et al.* (2010), d is from Bao *et al.* (2009).

Reference

Baski, A.K., Hsu, V., McWilliams, M.O. & Farrar, E. 1992. $^{40}Ar/^{39}Ar$ dates of the Brunhes-Matuyama geomagnetic field reversal. Science, 256, 356-357.

Baksi, A.K. 2003. Critical evaluation of $^{40}Ar/39Ar$ ages for the central Atlantic magmatic province: timing, duration and possible migration of magmatic centers. In: Hames, W.E., McHone, J.G., Renne, P.R., Ruppel, C. (Eds.), The Central Atlantic Magmatic Province: Insights from Fragments of Pangaea, 136. American Geophysical Union Monograph, Washington D.C, pp. 77–90.

Baksi, A.K. 2007a. A quantitative tool for detecting alteration in undisturbed rocks and minerals -I: water, chemical weathering and atmospheric argon. In: Foulger, G.R., Jurdy, D.M. (Eds.), Plates, plumes and planetary processes: Geological Society of America Special Paper, 430, 285–303.

Baksi, A.K. 2007b. A quantitative tool for detecting alteration in undisturbed rocks and minerals - II: application to argon ages related to hotspots. In: Foulger, G.R., Jurdy, D.M. (Eds.), Plates, plumes and planetary processes: Geological Society of America Special Paper, 430, 305–333.

Baksi, A.K. 2012. New $^{40}Ar/^{39}Ar$ dates of the Grande Ronde lavas, Columbia River Basalts, USA: Implications for duration of flood basalt eruption episodes" by Barry et al. (2010)-Discussion. Lithos, 146, 293–299.

Baksi, A.K. 2013. Timing and duration of volcanism in the Columbia River Basalt Group: A review of existing radiometric data and new constraints on the age of the Steens through Wanapum Basalt extrusion. Geological Society of America Special Paper, 497, 67–85.

Baksi, A.K. 2014a. The Deccan Trap-Cretaceous-Paleogene boundary connection; new 40Ar/39Ar ages and critical assessment of existing argon data pertinent to this hypothesis. Journal of Asian Earth Sciences, 84, 9-23.

Baksi, A.K. 2014b. $^{40}Ar/^{39}Ar$ ages of flood basalts provinces in Russia and China and their possible link to global faunal extinction events: a cautionary tale regarding alteration and loss of 40Ar*. Journal of Asian Earth Sciences, 84, 118-130.

Bao, P.S., Su, L., Zhai, Q.G. & Xiao, X.C. 2009. Compositions of the kimberlitic brecciated peridotite in the Bachu area, Xijiang and its ore-bearing potentialities. Acta Geologica Sinica, 83, 1276–1301. (in Chinese with English abstract)

Berry, R.F., Jenner, G.A., Meffre, S. & Tubrett, M.N. 2001. A North American provenance for Neoproterozoic to Cambrian sandstones in Tasmania? Earth and Planetary Science Letters 192 207-222.

Barboni, M., Schoene, B., Ovtcharova, M., Bussy, F., Schaltegger, U. & Gerdes, A. 2013. Timing of incremental pluton construction and magmatic activity in a back-arc setting revealed by ID-TIMS U/Pb and Hf isotopes on complex zircon grains. Chemical Geology, 342, 76-93.

Beyer, C., Berndt, J., Tappe, S. & Klemme, S. 2013. Trace element partitioning between perovskite and kimberlite to carbonatite melt: new experimental constraints. Chemical Geology, 353, 132–139.

Boehnke, P., Watson, E. B., Trail, D., Harrison, T. M. & Schmitt, A. K. 2013. Zircon saturation re-revisited. Chemical Geology, 351, 324-334.

Becker, M. & Le Roex, A.P. 2006. Geochemistry of South African on- and off-craton, Group I and Group II kimberlites: petrogenesis and source region evolution. Journal of Petrology, 47 (4), 673–703.

Chen, M.M., Tian, W., Zhang, Z.L. & Guan, P. 2010. Geochronology of the Permian basic-intermediate-acidic magma suite from Tarim, northwest China and its geological implications. Acta Petrologica Sinica, 26, 559-572. (in Chinese with English abstract)

Cherniak, D.J. & Watson, E.B. 2001. Pb diffusion in zircon. Chemical Geology, 172, 5–24.

Davies, G. R., Spriggs, A. J. & Nixon, P. H. 2001. A non-cognate origin for the Gibeon kimberlite megacryst suite, Namibia: implications for the origin of Namibian kimberlites. Journal of Petrology, 42(1), 159-172.

DeVor, R.E., Chang, T-H. & Sutherland, J.W. 1992. Statistical quality design and control, Prentice-Hall, Upper Saddle River, New Jersey, 787-797.

Dickinson, W. R. & Gehrels, G. E. 2009. Use of U–Pb ages of detrital zircons to infer maximum depositional ages of strata: a test against a Colorado Plateau Mesozoic database. Earth and Planetary Science Letters, 288(1), 115-125.

Donatti-Filho, J. P., Tappe, S., Oliveira, E. P. & Heaman, L. M. 2013. Age and origin of the Neoproterozoic Brauna kimberlites: Melt generation within the metasomatized base of the São Francisco craton, Brazil. Chemical Geology, 353, 19-35.

Du, P.L. 1983. Brief introduction of geological characters of kimberlite body at Wajilitag in Bachu County, Xinjiang. Xinjiang Geology 1, 55-64. (in Chinese with English abstract)

Duncan, R.A., Hooper, P.R., Rehacek, J., Marsh, J.S. & Duncan, A.R. 1997. The timing and duration of the Karoo igneous event, southern Gondwana. Journal of Geophysical Research [Solid Earth], 102, 18127-18138.

Gagnevin, D., Daly, J. S. & Kronz, A. 2010. Zircon texture and chemical composition as a guide to magmatic processes and mixing in a granitic environment and coeval volcanic system. Contributions to Mineralogy and Petrology, 159(4), 579-596.

Gehrels, G.E., Valencia, V.A. & Ruiz, J. 2008. Enhanced precision, accuracy, efficiency, and spatial resolution of U-Pb ages by laser ablation-multicollector-inductively coupled plasma-mass spectrometry: Geochemistry, Geophysics, Geosystems, 9, 1-13.

Gehrels, G.E. 2012. Detrital zircon U-Pb geochronology: Current methods and new opportunities, *in* Busby, C. and Azor, A., eds., Tectonics of sedimentary basins: Recent advances: West Sussex, John Wiley & Sons, 45-62. doi:10.1002/9781444347166.ch2

Grimes, C.B., John, B.E., Cheadle, M.J., Mazdab, F.K., Wooden, J.L., Swapp, S. & Schwartz, J.J. 2009. On the occurrence, trace element geochemistry, and crystallization history of zircon from in situ ocean lithosphere. Contributions to Mineralogy and Petrology, 158(6), 757-783.

Harris, M., Le Roex, A. & Class, C. 2004. Geochemistry of the Uintjiesberg kimberlite, South Africa: petrogenesis of an off-craton, group I, kimberlite. Lithos, 74 (3–4), 149–165.

Heaman, L.M. 1989. The nature of the subcontinental mantle from Sr-Nd-Pb isotopic studies on kimberlitic perovskite. Earth and Planetary Science Letters, 92(3-4), 323-334.

Heaman, L.M. & Kjarsgaard, B.A. 2000. Timing of eastern North American kimberlite magmatism: continental extension of the Great Meteor hotspot track? Earth and Planetary Science Letters, 178, 253–268.

Huang, H., Zhang, Z.C., Kusky, T., Santosh, M., Zhang, S., Zhang, D.Y., Liu, J.L. & Zhao, Z.D. 2012. Continental vertical growth in the transitional zone between South Tianshan and Tarim, western Xinjiang, NW China: Insight from the Permian Halajun A1-type granitic magmatism. Lithos, 155, 49–66.

Jerram, D. A. & Widdowson, M. 2005. The anatomy of Continental Flood Basalt Provinces: geological constraints on the processes and products of flood volcanism. Lithos, 79(3), 385-405.

Jia, C.Z. 1997. Tectonic Characteristics and Oil-Gas, TarimBasin. Petroleum Industry Press, China, Beijing (in Chinese).

Jiang, C.Y., Zhang, P.B., Lu, D.R., Bai, K.Y., Wang, Y.P., Tang, S.H., Wang, J.H. & Yang, C. 2004a. Petrology, geochemistry and petrogenesis of the Kalpin basalts and their Nd, Sr and Pb isotopic compositions. Geology Review, 50(5), 492–500. (in Chinese with English abstract)

Jiang, C.Y., Zhang, P.B., Lu, D.R. & Bai, K.Y. 2004b. Petrogenesis and magma source of the ultramafic rocks at Wajilitag region, western Tarim Plate in Xinjiang. Acta Geologica Sinica, 20, 1433–1444. (in Chinese with English abstract)

Jiang, C.Y., Jia, C.Z., Li, L.C., Zhang, P.B., Lu, D.R. & Bai, K.Y. 2004c. Source of the Fe-enriched type high-Mg magma in Mazhartag region, Xinjiang. Acta Geologica Sinica, 78, 770–780. (in Chinese with English abstract)

Kaczmarek, M.A., Müntener, O. & Rubatto, D. 2008. Trace element chemistry and U–Pb dates of zircons from oceanic gabbros and their relationship with whole rock composition (Lanzo, Italian Alps). Contributions to Mineralogy and Petrology, 155(3), 295-312.

Katayama, I., Muko, A., Lizuka, S., Terada, K., Tsutsuimi, Y., San, Y., Zhang, R.Y. & Liou, J.G. 2003. Dating of zircon from Ticlinohumite-bearing garnet peridotite: implication for timing of mantle metasomatism. Geology, 31, 713–716.

Kemp, A.I.S., Wormald, R.J., Whitehouse, M.J. & Price, R.C. 2005. Hf isotopes in zircon reveal contrasting sources and crystallization histories for alkaline to peralkaline granites of Temora, southeastern Australia. Geology, 33(10), 797-800.

Le Maitre, R.W. (ed.) 2002. Igneous Rocks. A Classification and Glossary of Terms. Recommendations of the International Union of Geological Sciences Subcommission on the Systematics of Igneous Rocks, 2nd ed. xvi + 236 pp. Cambridge, New York, Melbourne: Cambridge University Press.

Le Roex, A.P., Bell, D.R. & Davis, P. 2003. Petrogenesis of group I kimberlites from Kimberley, South Africa: evidence from bulk-rock geochemistry. Journal of Petrology, 44 (12), 2261–2286.

Lo, C.H., Chung, S.L., Lee, T.Y. & Wu, G. 2002. Age of the Emeishan flood magmatism and Permo-Triassic boundary events. Earth and Planetary Science Letters 198, 449–458.

Liang, R.X. & Fang, Q.S. 1991. The new insights of Wajilitag "kimberlite" in Bachu, Xinjiang. Geological Review, 37, 95-96. (in Chinese).

Liu, H.Q., Xu, Y.G., Tian, W., Zhong, Y.T., Mundil, R., Li, X.H. & Shangguan, S. M. 2014. Origin of two types of rhyolites in the Tarim Large Igneous Province: Consequences of incubation and melting of a mantle plume. Lithos, 204, 59-72

Li, C.N., Lu, F.X. & Chen, M.H. 2001. Research on petrology of the Wajilitag complex body in north edge in the Tarim Basin. Xinjiang Geology 19 (1), 38–43. (in Chinese with English abstract)

Li, H.Y., Huang, X.L., Li, W.X., Cao, J., He, P.L. & Xu, Y.G. 2013. Age and geochemistry of the Early Permian basalts from Qimugan in the southwestern Tarim basin. Acta Petrological Sinica, 29(10), 3353-3368. (in Chinese with English abstract).

Li, Y., Su, W., Kong, P., Qian, Y.X., Zhang, K.L., Zhang, M.L., Chen, Y., Cai, X.Y. & You, D.H. 2007. Zircon U–Pb ages of the Early Permian magmatic rocks in the Tazhong–Bachu region, Tarim Basin by LA-ICP-MS. Acta Petrologica Sinica, 23(5), 1097–1107. (in Chinese with English abstract)

Li, Y.Q., Li, Z.L., Sun, Y.L., Chen, H.L., Yang, S.F. & Yu, X. 2010. PGE and geochemistry of Wajilitag ultramafic cryptoexplosive brecciated rocks from Tarim Basin: implications for petrogenesis. Acta Petrologica Sinica, 26, 3307–3318. (in Chinese with English abstract)

Li, Y.Q. 2013. Study on magma dynamics and ore potential of the Early Permian Tarim large igneous province. Ph.D. Dissertation. Hangzhou: Zhejiang University, 1-122. (in Chinese with English summary)

Li, Y.Q., Li, Z.L., Yu, X., Santosh, M., Langmuir, C.H., Yang, S.F., Chen, H.L., Tang, Z.L., Song, B. & Zou, S.Y. 2014a. Origin of the Early Permian zircons in Keping basalts and magma evolution of the Tarim Large Igneous Province (northwestern China). Lithos, 204, 47-58.

Li, Z.L., Yang, S.F., Chen, H.L., Langmiur, C.H., Yu, X., Lin, X.B. & Li, Y.Q. 2008. Chronology and geochemistry of Taxinan basalts from the Tarim Basin: evidence for Permian plume magmatism. Acta Petrologica Sinica, 24(5), 959–970. (in Chinese with English abstract)

Li, Z.L., Chen, H.L., Song, B., Li, Y.Q., Yang, S.F. & Yu, X. 2011. Temporal evolution of the Permian large igneous province in Tarim Basin, Northwest China. Journal of Asian Earth Sciences, 42, 917–927.

Li, Z.L., Li, Y.Q., Chen, H.L., Santosh, M., Yang, S.F., Xu, Y.G., Langmuir, C.H., Chen, H.L., Yu, X. & Zou, S.Y. 2012. Hf isotopic characteristics of the Tarim Permian large igneous province rocks of NW China: Implication for the magmatic source and evolution. Journal of Asian Earth Sciences, 49, 191-202.

Ludwig, K. R. 1998. On the treatment of concordant uranium-lead ages. Geochimica et Cosmochimica Acta, 62(4), 665-676.

Ludwig, K.R. 2008. Isoplot 3.6: Berkeley Geochronology Center Special Publication 4, 77.

Luo, J. H., Che, Z. C., Zhou, N. C., Yang, W., Song, H. X., Hou, X. J. & Han, K. 2013. Geochemistry and isotopic geochronology of dacites from the Lower Permian Xiaotikanlike Formation in the southern margin of South Tianshan, and its tectonic significances. Acta Geologica Sinica, 87 (1), 29–37 (in Chinese with English abstract).

Marzoli, A., Renne, P.R., Piccirillo, E.M., Ernesto, M., Bellieni, G. & De Min, A. 1999. Extensive 200-million year old continental flood basalts of the Central Atlantic Magmatic Province. Science, 284, 616–618.

Mattinson, J. M. 1987. U-Pb ages of zircons: A basic examination of error propagation. Chemical Geology: Isotope Geoscience section, 66(1), 151-162.

Mattinson, J. M. 2005. Zircon U–Pb chemical abrasion ("CA-TIMS") method: combined annealing and multi-step partial dissolution analysis for improved precision and accuracy of zircon ages. Chemical Geology, 220(1), 47-66.

Melluso, L., Lustrino, M., Ruberti, E., Brotzu, P., de Barros Gomes, C., Morbidelli, L., Morra, V., Svisero, D. P. & d'Amelio, F. 2008. Major-and trace-element composition of olivine, perovskite, clinopyroxene, Cr–Fe–Ti oxides, phlogopite and host kamafugites and kimberlites, Alto Paranaiba, Brazil. The Canadian Mineralogist, 46(1), 19-40.

Memeti, V., Paterson, S., Matzel, J., Mundil, R. & Okaya, D. 2010. Magmatic lobes as "snapshots" of magma chamber growth and evolution in large, composite batholiths: An example from the Tuolumne intrusion, Sierra Nevada, California. Geological Society of America Bulletin, 122(11-12) 1912-1931.

Mezger, K. & Krogstad, E.J. 1997. Interpretation of discordant U–Pb zircon ages: An evaluation. Journal of Metamorphic Geology, 15, 127–140.

Michel, J., Baumgartner, L., Putlitz, B., Schaltegger, U. & Ovtcharova, M. 2008. Incremental growth of the Patagonian Torres del Paine laccolith over 90 ky. Geology, 36(6), 459-462.

Miller, C. F., McDowell, S. M. & Mapes, R. W. 2003. Hot and cold granites? Implications of zircon saturation temperatures and preservation of inheritance. Geology, 31(6), 529-532.

Miller, J. S., Matzel, J. E., Miller, C. F., Burgess, S. D. & Miller, R. B. 2007. Zircon growth and recycling during the assembly of large, composite arc plutons. Journal of Volcanology and Geothermal Research, 167(1), 282-299.

Mitchell, R. H. 2008. Petrology of hypabyssal kimberlites: relevance to primary magma compositions. Journal of Volcanology and Geothermal Research, 174(1), 1-8.

Patterson, M., Francis, D. & McCandless, T. 2009. Kimberlites: magmas or mixtures? Lithos, 112, 191–200.

Qin, K.Z., Su, B.X., Sakyi, P.A., Tang, D.M., Li, X.H., Sun, H., Xiao, Q.H. & Liu, P.P. 2011. SIMS zircon U–Pb geochronology and Sr-Nd isotopes of Ni–Cu-bearing mafic–ultramafic intrusions in eastern Tianshan and Beishan in correlation with flood basalts in Tarim Basin (NW China): constraints on a ca. 280 Ma mantle plume. American Journal of Science, 311, 237–260.

R Development Core Team. 2008. R: A Language and Environment for Statistical Computing, R Foundation for Statistical Computing, Vienna, Austria, ISBN 3-900051-07-0.

Riishuus, M. S., Peate, D. W., Tegner, C., Wilson, J. R., Brooks, C. K. & Harris, C. 2006. Temporal evolution of a long-lived syenitic centre: the Kangerlussuaq Alkaline Complex, East Greenland. Lithos, 92(1), 276-299.

Sarkar, C., Storey, C.D., Hawkesworth, C.J. & Sparks, R.S.J. 2011. Degassing in kimberlite: oxygen isotope ratios in perovskites from explosive and hypabyssal kimberlites. Earth and Planetary Science Letters, 312(3–4), 291–299.

Sarkar, C., Storey, C. D. & Hawkesworth, C. J. 2014. Using perovskite to determine the pre-shallow level contamination magma characteristics of kimberlite. Chemical Geology, 363, 76-90.

Schaltegger, U., Brack, P., Ovtcharova, M., Peytcheva, I., Schoene, B., Stracke, A., Marocchi, M. & Bargossi, G. M. 2009. Zircon and titanite recording 1.5 million years of magma accretion, crystallization and initial cooling in a composite pluton (southern Adamello batholith, northern Italy). Earth and Planetary Science Letters, 286(1), 208-218.

Schmitz, M. D. & Schoene, B. 2007. Derivation of isotope ratios, errors, and error correlations for U-Pb geochronology using ^{205}Pb-^{235}U-(^{233}U)-spiked isotope dilution thermal ionization mass spectrometric data. Geochemistry, Geophysics, Geosystems, 8(8).

Schoene, B., Guex, J., Bartolini, A., Schaltegger, U. & Blackburn, T. J. 2010. Correlating the end-Triassic mass extinction and flood basalt volcanism at the 100 ka level. Geology, 38(5), 387-390.

Schoene, B., Condon, D. J., Morgan, L. & McLean, N. 2013. Precision and accuracy in geochronology. Elements, 9(1) 19-24.

Schoene, B. 2014. U-Th-Pb Geochronology, in Treatise on Geochemistry 2nd Edition, ch. 3.10, Rudnick R, ed.

Sharp, W.D. & Clague, D.A. 2006. 50-Ma initiation of the Hawaiian-Emperor Bend records major change in Pacific plate motion. Science, 313, 1281–1284.

Sircombe, K.N. 1999. Tracing provenance through the isotope ages of littoral and sedimentary detrital zircon, eastern Australia. Sedimentary Geology, 124, 47-67.

Sparks, R. 2013. Kimberlite Volcanism. Annual Review of Earth and Planetary Sciences, 41, 497–528.

Stuart, P. L. 1982. Least squares quantization in PCM. IEEE Transactions on Information Theory, IT-28, 129–137.

Su, L. 1991. A research on magmatic inclusions in minerals from kimberlite in Bachu County, Xinjiang, China. Periodical of Xi'an Geological Mineral Institute, 32, 15–33. (in Chinese).

Sun, S. S. & McDonough, W. 1989. Chemical and isotopic systematics of oceanic basalts: implications for mantle composition and processes. Geological Society of London Special Publications, 42(1), 313-345.

Sun, L.H., Wang, Y.J., Fan, W.M. & Zi, J.W. 2008. A further discussion of the petrogenesis and tectonic implication of the Mazhashan syenites in the Bachu area. Journal of Jilin University (Earth Science Edition), 38(1), 8-20. (in Chinese with English abstract)

Sun, Y., Xiao, Y.F., Zhao, X.K., Qian, Y.X., Xiao, G.W. & Liu, H.Q. 2009. The zircon U-Pb age of Mazha'erTage alkalic complex in the Tarim Basin and its geologic significance. Acta Geologica Sinica, 83(6), 775-781. (in Chinese with English abstract)

Tian, W., Campbell, I.H., Allen, C., Guan, P., Pan, W., Chen, M.M., Yu, H. & Zhu. W. P. 2010. The Tarim picrate-basalt-rhyolite suite, a Permian flood basalt from northwest China with contrasting rhyolites produced by fractional crystallization and anatexis. Contributions to Mineralogy and Petrology, 160 (3), 407-425.

Wang, Y.S. & Su, L. 1987. Petro-mineral characteristics of Wajilitag kimberlites and contrast with some correlation region, Bachu, Xinjiang. Periodical of Xi'an Geological Mineral Institute, 15, 47-56. (in Chinese)

Wang, Y.S. & Su, L. 1990. Composition characteristics and forming condition of phlogolites in Wajilitage kimberlites, Bachu, Xinjiang. Periodical of Xi'an Geological Mineral Institute, 28, 47-55. (in Chinese)

Watson, E. B. & Harrison, T. M. 1983. Zircon saturation revisited: temperature and composition effects in a variety of crustal magma types. Earth and Planetary Science Letters, 64(2), 295-304.

Wendt, I. & Carl, C. 1991. The statistical distribution of the mean squared weighted deviation. Chemical Geology: Isotope Geoscience Section, 86(4), 275-285.

Wei, X. & Xu, Y.G. 2011. Petrogenesis of Xiaohaizi syenite complex from Bachu area, Tarim. Acta Petrologica Sinica, 27(10), 2984- 3004. (in Chinese with English abstract)

Wei, X. & Xu, Y.G. 2013. Petrogenesis of the mafic dykes from Bachu and implications for the magma evolution of the Tarim large igneous province, NW China. Acta Petrologica Sinica, 29(10), 3323- 3335. (in Chinese with English abstract)

Wei, X., Xu, Y.G., Feng, Y.X. & Zhao, J.X. 2014. Plume–lithosphere interaction in the generation of the Tarim large igneous province, NW China: geochronological and geochemical constraints. American Journal of Science, 314, 314–356.

Wu, G.H., Li, H.W., Xu, Y.L., Su, W., Chen, Z.Y. & Zhang, B.S. 2012. The tectonothermal events, architecture and evolution of Tarim craton basement palaeo-uplifts. Acta Petrologica Sinica, 28(8), 2435 — 2452. (in Chinese with English abstract)

Xu, Y.G., Wei, X., Luo, Z.Y., Liu, H.Q. & Cao, J. 2014. The Early Permian Tarim Large Igneous Province: Main characteristics and a plume incubation model. Lithos, 204, 20-35.

Yang, S.F., Chen, H.L., Dong, C.W., Jia, C.Z. & Wang, Z.G. 1996. The discovery of Permian syenite inside Tarim Basin and its geodynamic significance. Geochimica, 25(2), 121-128. (in Chinese with English abstract).

Yang, S.F., Li, Z.L., Chen, H.L., Xiao, W.J., Yu, X., Lin, X.B. & Shi, X.G. 2006a. Discovery of a Permian quartz syenitic porphyritic dyke from the Tarim Basin and its tectonic implications. Acta Petrologica Sinica, 22 (5), 1405–1412. (in Chinese with English abstract)

Yang, S.F., Li, Z.L., Chen, H.L., Chen, W. & Yu, X. 2006b. $^{40}Ar/^{39}Ar$ dates of basalts from Tarim Basin, NW China and its implication to a Permian thermal tectonic event. Journal of Zhejiang University - Science A 7 (Supp. II), 170–174.

Yang, S.F., Li, Z.L. & Chen, H.L. 2007. Permian bimodal dyke of Tarim Basin, NW China: Geochemical characteristics and tectonic implications. Gondwana Research, 12, 113-120.

Yu, X. 2009. Magma evolution and seep geological processes of Early Permian Tarim Large Igneous Province. Ph.D. Dissertation. Hangzhou: Zhejiang University, 1-136. (in Chinese with English summary)

Yu, X., Yang, S.F., Chen, H.L., Chen, Z.Q., Li, Z.L., Batt, G.E. & Li, Y.Q. 2011b. Permian flood basalts from the Tarim Basin, Northwest China: SHRIMP zircon U-Pb dates and geochemical characteristics. Gondwana Research, 20(2-3), 485-497.

Zhang, H.A., Li, Y.J., Wu, G.Y., Su, W., Qian, Y.X., Meng, Q.L., Cai, X.Y., Han, L.J., Zhao, Y. & Liu, Y.L. 2009. Isotopic geochronology of Permian igneous rocks in the Tarim Basin. Chinese Journal of Geology, 44 (1), 137–158. (in Chinese with English abstract).

Zhang, C.L., Li, X.H., Li, Z.X., Ye, H.M. & Li, C.N. 2008a. A Permian layered intrusive complex in the Western Tarim Block, northwestern China: product of a Ca. 275–Ma mantle plume? Journal of Geology, 116 (3), 269–287.

Zhang, C.L., Xu, Y.G., Li, Z.X., Wang, H.Y. & Ye, H.M. 2010a. Diverse Permian magmatism in the Tarim Block, NW China: Genetically linked to the Permian Tarim mantle plume? Lithos, 119 (3-4): 537-552.

Zhang, C.L. & Zou, H.B. 2013. Permian A-type granites in Tarim and western part of Central Asian Orogenic Belt (CAOB): Genetically related to a common Permian mantle plume? Lithos, 172, 47-60.

Zhang, D.Y., Zhang, Z.C., Santosh, M., Cheng, Z., He, H. & Kang, J. 2013. Perovskite and baddeleyite from kimberlitic intrusions in the Tarim large igneous province signal the onset of an end-Carboniferous mantle plume. Earth and Planetary Science Letters, 361, 238–248.

Zhang, Z.L., Qin, Q.M., Tian, W., Cao, B., Li, B.S. & Chen, M.M. 2008b. Emplacement characteristics and spatial distribution of Permian Mazhartager basic dike swarms in Bachu area, Tarim basin. Acta Petrologica Sinica, 24(10), 2273-2280 (in Chinese with English abstract).

Zhou, M.F., Zhao, J.H., Jiang, C.Y., Gao, J.F., Wang, W. & Yang, S.H. 2009. OIB–like, heterogeneous mantle sources of Permian basaltic magmatism in the western Tarim Basin, NW China: implications for a possible Permian large igneous province. Lithos, 113, 583–594.

Zou, S.Y., Li, Z.L., Ren, Z.Y., Li, Y.Q., Yang S.F., Chen, H.L., Song, B. & Yu, X. 2013. U-Pb dates and Hf isotopic compositions of the detrital zircons from Permian sedimentary rocks in Keping area of Tarim Basin, Xianjiang, China: Constraints on geological evolution of Tarim Block. Acta Petrologica Sinica, 29(10), 3369-3388. (in Chinese with English abstract).